Biophysical Chemistry 251 (2019) 106146

Contents lists available at ScienceDirect

Biophysical Chemistry

journal homepage: www.elsevier.com/locate/biophyschem

Temperature-dependence of the bending elastic constant of DNA and extension of the two-state model. Tests and new insights

J. Michael Schurr

Department of Chemistry, University of Washington, Box 351700, United States

HIGHLIGHTS

- With increasing T from 278 to 315 K, the bending elastic constant of DNA rises, while the torsion elastic constant falls.
- Bending elastic constants of the a and b states of the previously formulated two-state cooperative transition model are estimated.
- The inverse torsion and inverse bending elastic constants are linearly anti-correlated as T is varied.
- The two-state model quantitatively accounts for observations from diverse single-molecule and ensemble experiments.
- The broad premelting transition of DNA likely arises from this T-dependent shift of the two-state equilibrium.

GRAPHICAL ABSTRACT

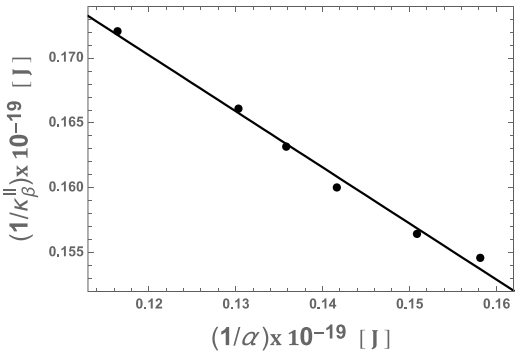

ABSTRACT

Review and analyses of the experimental data indicate that in nearly all cases bending elastic constants of the effective springs between bp of DNA actually undergo a net increase with increasing T from 278 to 315 K. The exceptions to this rule are bending elastic constants obtained from equilibrium topoisomer distributions of a 2686 bp pUC19 DNA by *assuming* a fixed T-independent value of the torsion elastic constant. When the same data are analyzed using *measured* T-dependent values of the torsion elastic constant, which decline with increasing T, a modest increase in bending elastic constant with increasing T is obtained. After revising the torsion elastic constants of the previously formulated two-state cooperative transition model to account for additional data, that model is fitted to the bending elastic constants reckoned from the aforementioned topoisomer distributions to determine the best-fit values for each state. The rather good fit implies a strong negative linear correlation between the inverse bending and inverse torsion elastic constants as T is varied. Predictions of the resulting two-state model, wherein each state has fixed bending and torsion elastic constants, agree surprisingly well with single-molecule relative extension and torque data. The same model also yields good agreement with numerous other experimental data. With increasing T the equilibrium is shifted from the (longer, torsionally stiffer, flexurally softer) b-state toward the (shorter, torsionally softer, flexurally stiffer) a-state. This transition is suggested to be the origin of the so-called broad pre-melting transition exhibited by many, but not all, DNAs.

1. Introduction

The responses of a DNA molecule to imposed constraints or applied mechanical stresses are governed largely by the torsion and bending elastic constants, α (J) and κ_β (J), respectively, of its effective springs between base-pairs, and its response to tension, which at low forces was recently suggested to induce a highly cooperative transition between two conformations of different length [1,2]. In that case, the effective

E-mail address: jmschurr@zipcon.com.

https://doi.org/10.1016/j.bpc.2019.106146
Received 16 February 2019; Received in revised form 28 March 2019; Accepted 1 April 2019
Available online 08 April 2019

spring is the resistance to shifting the prevailing equilibrium between the two coexisting conformations. The strengths of these springs together with the inter-duplex interaction potential determine the free energy change that accompanies any change in constraint (e.g. circularization or a change of linking difference) or mechanical stress (e.g. tension or torque) at constant temperature. Such information is essential for calculating the deformational free energy contribution to the total free energy change and equilibrium constant to form particular DNA configurations either alone or in DNA/protein complexes.

The commonly used bending rigidity, $A = h\kappa_\beta$ (Jm), and twisting rigidity, $C = h\alpha$ (Jm), where h (nm) is the rise per bp, are in a sense secondary, because recent evidence strongly suggests that unstressed DNAs exhibit two (or more) distinct conformations, which exhibit modestly different values of h [3–5] and as much as ~2.9-fold different values of α [1,2,6–8]. Hence, it is often preferable to focus on the effective springs between base-pairs (bp), whose number N is fixed, and their elastic constants, which do not depend upon the value of h. Previous discussions of κ_β have usually been couched in terms of the persistence length, a statistical quantity that contains contributions to the mean squared curvature not only from thermally excited elastic bends but also from any sequence-dependent static or average bends [9–11]. The persistence length for an *intrinsically straight* DNA is accurately approximated by, $P = h_{av}\kappa_\beta/k_BT$, where h_{av} is the average tension- and T-dependent rise per base-pair (bp) along the helix axis, k_B is Boltzmann's constant, and T is absolute temperature. The value of κ_β extracted from P for a DNA that is not intrinsically straight using the above relation is necessarily an *apparent* value that contains contributions from sequence-dependent static bends (intrinsic curvature) as well as from thermally excited bending and stretching springs [11].

Evidence for (1) polymorphism of DNAs of both natural and synthetic sequences; (2) for highly cooperative (long-range) allosteric transitions between different duplex states of DNA caused by local changes in sequence and structure; and (3) for involvement of such transitions in the action of remotely bound transcriptional enhancers was reviewed in 1998 [12]. A more detailed account of the early evidence obtained by fluorescence methods appeared in 1992 [13]. More recent evidence for cooperative transitions between two (or more) duplex structures comes from X-ray scattering measurements on 10–35 base-pair (bp) DNAs specifically labeled with gold colloids [3–5], from analyses [1] of relative extension vs. force measurements on single untwisted DNAs [6], and from analyses [1] of torque vs. force measurements on single twisted DNAs under tension [6,7]. A model of a cooperative transition between two states, a and b, within the B-family with different rises per bp and different torsion elastic constants was previously formulated. By assuming that P remained constant at 50 nm under the prevailing conditions, relevant model parameters, such as the difference in rise per bp between the two states, the cooperativity parameter, J, the equilibrium constant, B_0, for the $a \Leftrightarrow b$ transition of an isolated bp under the prevailing conditions, and the torsion elastic constants, α_a and α_b, of the effective springs between bp of the two states, were quantitatively estimated [1].

1.1. Plan of the paper

The purposes of this paper are: (i) to identify the *increasing* trend of κ_β with increasing temperature, and resolve a notable discrepancy pertaining to that; (ii) to determine the respective $\kappa_{\beta a}$ and $\kappa_{\beta b}$ values of the a and b states; (iii) to slightly revise the torsion elastic constants α_a and α_b of the model by including three recent torque measurements [14] and a datum at higher force [7] in the fitting process, and to test the model more directly and broadly than heretofore; (iv) to illuminate the negative linear correlation between $1/\kappa_\beta$ and $1/\alpha$ with varying T, which is consistent with a shift of the $a \Leftrightarrow b$ equilibrium toward the a state with increasing T; (v) to examine the possibility that such a shift is the origin of the so-called broad premelting transition; and (vi) to resolve, or at least better understand, additional puzzles and discrepancies in the literature. This study is divided into sequential subsections as follows.

(1) Relevant literature regarding the variations of κ_β with temperature is briefly reviewed and critiqued. In the vast majority of cases, the average slope, $d\kappa_\beta/dT$, over the range 278 to 315 K was significantly *positive*, and in one case, $d\kappa_\beta/dT \cong 0$. However, κ_β values extracted by Geggier, Kotlyar, and Vologodskii (GKV) [15] from the measured free energy differences between topoisomers of a 2686 bp DNA by *assuming* a constant T-independent value of the torsion elastic constant, α, yielded a substantially *negative* average slope $d\kappa_\beta/dT$. Reanalyzing the same data in the same way, but using T-dependent values of α *measured* by Delrow, Heath, and Schurr (DHS) [16], which decline substantially with increasing T, yields κ_β values with a modest but significantly *positive* average slope $d\kappa_\beta/dT$, in agreement with the vast majority of other data.

(2) The two-state cooperative transition model with the previously determined [1] optimal parameter set 3 is adopted here, because its difference in rise per bp, $\delta = 0.0487$ nm, between the a and b states is closest to the recent estimate, $\delta = 0.05$ nm, from X-ray scattering studies of short DNAs specifically labeled with gold colloids [5]. (The previously published value, $\delta = 0.0467$ nm, for parameter set 3 was a typographical error.) Besides δ, parameter set 3 includes the cooperativity parameter, J, and the equilibrium constant, B_0, for the $a \Leftrightarrow b$ transition of an isolated bp, all of which were determined from relative extension vs. force data of Mosconi et al. [1,6], and remain unchanged. However, the corresponding values of α_a and α_b are slightly revised by fitting model 3 to a somewhat larger set of α-values, which were extracted from both old [6,7] and new [14] single molecule torque measurements at different forces by assuming that $P = 50$ nm and $h = 0.338$ nm under the prevailing conditions [1]. This revised model was used with the T-dependent α-values of DHS to reckon h at each T, which was then used to provide more refined values of the T-dependent κ_β and P at each T.

(3) The seemingly counterintuitive rise in κ_β with increasing T over the 278–315 K range is suggested to arise from a T-dependent shift of the two-state equilibrium away from the (longer and torsionally stiffer) b state, which is presumed to be *flexurally* softer, toward the (shorter and torsionally softer) a state, which is presumed to be *flexurally* stiffer, with increasing T. Importantly, both torsional and flexural (bending) elastic constants of the individual states are assumed to be constants independent of T over this limited range of temperatures. The $\kappa_{\beta a}$ and $\kappa_{\beta b}$ values associated with, respectively, the a and b states of the two-state model are obtained by least-squares fitting the model to the measured $1/\kappa_\beta$ values at various temperatures. Good quality of the resulting fit supports the premise that the decrease in $1/\kappa_\beta$ arises from the same shift in the two-state equilibrium that is associated with the increase in $1/\alpha$ with increasing T.

(4) The two-state model, which has evolved in stages, beginning with assumed fixed values of P and h, to one where P and h vary somewhat with both force and temperature, is tested directly against the primary data and then compared with numerous other experimental data, with surprisingly good agreement in all cases.

(5) The shift of the two-state cooperative equilibrium with increasing temperature from the (longer, torsionally stiffer, flexurally softer) b state toward the (shorter, torsionally softer, flexurally stiffer) a state over the range 278 to 315 K is suggested to be responsible for the so-called “broad premelting transition” transition of DNA that was extensively studied in the 1960s and 1970s by UV absorbance, circular dichroism (CD) [17–24], Raman [25], and IR [26] spectroscopies, and much later shown to be correlated with a decrease in the torsion elastic constant and increase in the bending elastic constant with increasing T [27].

(6) A comparison of the experimentally derived j-factors at different temperatures with theoretical values predicted by the cooperative

two-state model is undertaken, and the discrepancy between them discussed. Previously ignored problems with both *j*-factor measurements and *j*-factor calculations are analyzed in detail in the Supplementary Information. It is concluded that neither experimental *j*-factors nor theoretical predictions based upon an assumed circular ground state provide reliable estimates of the actual *j*-factors of small circular DNAs, so a satisfactory resolution of the discrepancy is presently not possible.

(7) The meaning and significance of the measured coarse-grained torsion and bending elastic constants are discussed.

(8) Important limitations of the two-state model are briefly noted.

In a paper currently in preparation the two-state model is applied to understand how a long-range allosteric transition in secondary structure could be induced by a particular change in sequence or structure over a very small region of a much longer DNA [12]. In that same paper, the two-state model with additional elaboration is also applied to reconcile discrepant results obtained for the contribution of intrinsic curvature to the persistence length of DNA by cryo-electron-microscopy on one hand and by *j*-factor measurements on the other [28,29].

2. Variation of κ_β with temperature

2.1. Sedimentation velocity measurements

From sedimentation studies of very long linear phage DNAs (in ~150 mM univalent cations), Gray and Hearst reported a ~1.05-fold increase in $S^0_{20,w}$ over the range from 278 to 322 K, from which they reckoned a ~0.90-fold decline in P [30]. This in turn implies a ~1.04-fold *increase* in κ_β over that same range, provided that h remains constant, and an even greater increase, if h should decrease with increasing T (as predicted below by the two-state model).

2.2. Electric dichroism measurements

Pörschke measured the terminal (longest) relaxation times in the off-field decays of the electric dichroism (ED) of several restriction fragments (43, 69, 84, 166, 179, 256 bp) in 100 mM Na^+ with and without 10 mM Mg^{2+} at temperatures of 275, 283, and 293 K [31]. These were analyzed both globally and individually using a combined Hagerman-Zimm [32]/Tirado-Garcia de la Torre [33] approach to estimate their persistence lengths and hydrodynamic cylinder radii. The global analyses indicated that *increasing* T from 275 to 293 K caused a 1.23-fold *increase* in P in the buffer without Mg^{2+}, and a similar 1.17-fold *increase* in P in the buffer with 10 mM Mg^{2+}. This trend in P is opposite that reported by both GKV[15] and Gray and Hearst [30], and implies an even faster rise of κ_β with increasing T than was found for the DNAs of Gray and Hearst.

The effect on P of adding 10 mM Mg^{2+} in the presence of 100 mM Na^+ was very slight at 293 K (< 1.01-fold increase), although it was larger at lower temperatures.

Analyses of three individual restriction fragments (166, 179, 256 bp) (in 100 mM Na^+ plus 10 mM Mg^{2+}) indicated that P *increased* with increasing T from 275 to 293 K for the first two fragments, but *decreased* for the 256 bp fragment. For the first two fragments, κ_β increased with increasing T, whereas κ_β of this 256 bp fragment remained constant within experimental uncertainty over this same range. These observations indicate a significant sequence-dependence of the slopes, dP/dT and $d\kappa_\beta/dT$, under the prevailing conditions.

Terminal relaxation times of a 95 bp DNA (in 2.4 mM Na^+), scaled accurately as T/η, where η is the solution viscosity, over the range 275 to 313 K. This implies that the persistence length of this fragment is practically constant and that the implied κ_β *increases* by 1.14-fold over this entire range [34].

2.3. Electric birefringence measurements

Lu et al. measured terminal relaxation times in the off-field decays of the electric birefringence (EB) of 15 restriction fragments (79 to 789 bp) in extremely low ionic strength (≤1 mM univalent cations) buffers, and analyzed those using several theoretical models to estimate the optimum persistence lengths and hydrodynamic radii for each [35]. These fragments all exhibited normal mobilities in gel electrophoresis at 293 K, and were presumed to lack substantial permanent bends. The global best-fit values of P and hydrodynamic radius for this set of fragments (in ~1 mM Tris plus 0.032 mM Na^+) were determined for each theoretical model at six different temperatures from 277 to 316 K. For every choice of model, P was found to *increase* significantly with increasing T from 4 to 20C, before *declining* with a further increase in T from 293 to 316 K. The model of Hagerman-Zimm [32]/Newman [36] gave the best overall fit, and indicated a ~1.15-fold *increase* in P from 277 to 293 K, similar to the global results from the ED studies at much higher ionic strength, before undergoing a 0.91-fold *decline* from 293 to 316 K. Despite the decline from 293 to 316 K, the *net* change in P over the entire range from 277 to 316 K is a 1.05-fold overall *increase*, which implies an *average* positive slope, $dP/dT > 0$, over the entire range. Interestingly, the 0.91-fold decline in P from 293 to 316 K is only very slightly steeper than the 0.927-fold decline expected for a constant value of κ_β, and within experimental error is compatible with that. These findings imply that the average slope $d\kappa_\beta/dT$ over the full 277–316 range of T is not only positive but also greater than that for the DNAs of Gray and Hearst. Analyses performed for several individual fragments indicated significant variation between fragments, although all fragments exhibited a maximum in P somewhere in the 293 to 316 K range. Although some of the observed trends might be specific to the extremely low prevailing salt concentrations in this TEB study [35], the increase in P from 277 to 293 K is similar to that observed by Pörschke [31] from 275 to 293 K for several DNAs in ~0.1 M univalent ionic strength and likely has similar origins.

2.4. Dynamic light scattering measurements

Dynamic light scattering (DLS) studies of Wilcoxon and Schurr (WS) [37] yielded center-of-mass translational diffusion coefficients for linear phage ϕ29 DNA (19,285 bp) (in ~110 mM univalent cations) over the range from 0 to 70 °C (273 to 343 K). After correction to 20,w conditions, those translational diffusion coefficients, $D_{20,w}(T)$, exhibited practically no significant variation with T over that entire range. Any relative increase in $D_{20,w}(T)$ with increasing T was significantly smaller than the relative increases in $S^0_{20,w}$ reported by Gray and Hearst [30].

In order to quantitatively compare the P vs. T curve of GKV with the DLS data of WS, it is necessary to transform values of P into translational diffusion coefficients under 20,w conditions. The theory of Yamakawa and Fujii (YF) [38] is most suitable for this purpose, but close agreement between the individual predicted values of $D_{20,w}(T)$ and the experimental values is not expected for two reasons. (1) A straight-line extrapolation of the experimental $D_{app}(q)$ to $q^2 = 0$, where q is the scattering vector, was used at all temperatures to minimize *relative* errors in $D_{app}(0)$ at the expense of modest underestimation of the absolute values of $D_{app}(0)$. (2) It is well known that YF theory requires a somewhat too large value of P, namely 65 nm, instead of a value nearer to 50 nm, in order to correctly predict absolute values of sedimentation coefficients of large DNAs at 293 K. Nevertheless, with an appropriate choice of persistence length (P = 65 nm) and a reasonable hydrodynamic diameter (2.5 nm), YF theory, which takes no account of self-interactions, exhibits remarkably close quantitative agreement with measured sedimentation coefficients over an extremely wide range of DNA sizes extending from 1500 bp, near the free-draining limit, where the diffusion coefficient is largely insensitive to moderate relative changes in P, to 1.5×10^6 bp [38], well into the range where self-interactions are highly significant [39]. This good agreement over

such a wide range of DNAs is believed to be due to "swelling" of the DNA "coil" by electrostatic self-repulsions. This suggests that the effect of excluded volume forces is to diminish or direct bending fluctuations in a manner that is in a practical sense equivalent to increasing its persistence length from 50 to 65 nm. Fortunately, the *ratio* of diffusion coefficients predicted for ϕ29 DNA by using a hydrodynamic diameter $d = 2.5$ nm with first $P_1 = 50$ nm and second with $P_2 = (0.60)$ $P_1 = 30$ nm, namely $D_2/D_1 = 1.218$, is very close to the *ratio* predicted for the same DNA by using first $P_3 = 65$ nm and second $P_4 = (0.60)$ $P_3 = 39$ nm, namely $D_4/D_3 = 1.206$ nm. In other words, for persistence lengths in the range of interest here (50 to 65 nm), the *ratio* of predicted diffusion coefficients, D_T^{GKV}/D_{273}^{GKV} for a given *ratio* (0.6) of persistence lengths is remarkably insensitive to the individual values of the persistence length at 273 K. Since we are interested primarily in the *T*-dependence of the *ratio*, P_T/P_{273}, it suffices to work with the corresponding variations in the ratio of diffusion coefficients, $D_{20,w}(T)/D_{20,w}(273)$, with increasing *T*.

A least-squares fit of the experimental $D_{20,w}^{exp}(T)$ values for the linear ϕ29 DNA (in ~110 mM univalent cations) by a straight line,

$$D_{20,w}^{line}(T) = a + b(T - 273) \quad (1)$$

yields, $a = (0.949 \pm 0.013)\text{x } 10^{-8}\,\text{cm}^2/\text{s}$ and $b = (-2.82 \pm 4.52)\text{ x } 10^{-12}\,\text{cm}^2/\text{s deg.}^{-1}$. A null slope, $b = 0$, lies well within the uncertainty range of *b*.

The *ratios* of diffusion coefficients computed from the best-fit straight line are,

$$D_{20,w}^{line}(T)/D_{20,w}^{line}(273) = 1.0 + (b/a)(T - 273)) \quad (2)$$

where the slope is $b/a = -2.98 \times 10^{-4}\,\text{deg.}^{-1}$, and its standard deviation is $\sigma_{b/a} = 5.04 \times 10^{-4}$. All standard deviations are obtained by conventional error propagation methods using the standard deviations of the measured $D_{20,w}(T)$ values, which are taken to be uniform and given by, $\sigma_D = 0.030 \times 10^{-8}\,\text{cm}^2/\text{s}$, which corresponds to 3.1 to 3.3% of the measured values. Again, a null slope, $b/a = 0$, lies well within the uncertainty $\sigma_{b/a}$ in b/a. In the sequel, Eq.2 is referred to as the *best-fit ratio line*.

The values of $D_{20,w}^{line}(T)$ and their ratios, $D_{20,w}^{line}(T)/D_{20,w}^{line}(273)$, are listed in Table 1. The experimental values of $D_{20,w}^{Exp}(T)$ and the corresponding ratios, $D_{20,w}^{Exp}(T)/D_{20,w}^{line}(273)$, are also listed in Table 1. Values of P_{GKV} were taken from the proposed curve of *P* vs. *T* in Fig. 7 of their paper, including a short linear extrapolation from 338 to 343 K, and listed in Table 1. The extrapolated value of P_{GKV} at 343 K is expected to be an upper bound, and to yield a lower bound for the $D_{20,w}^{GKV}(343)/D_{20,w}^{GKV}(273)$ ratio at that temperature. From the value of P_{GKV} at each temperature and an assumed DNA hydrodynamic diameter of 2.5 nm, the predicted friction coefficient for the 19,285 bp ϕ29 DNA was reckoned via Eqs. 49 and 50 of the YF paper [39], and converted to a 20,w diffusion coefficient, $D_{20,w}^{GKV}(T)$, in the standard way. The ratios of 20,w diffusion coefficients, $D_{20,w}^{GKV}(T)/D_{20,w}^{GKV}(273)$, are also listed in Table 1.

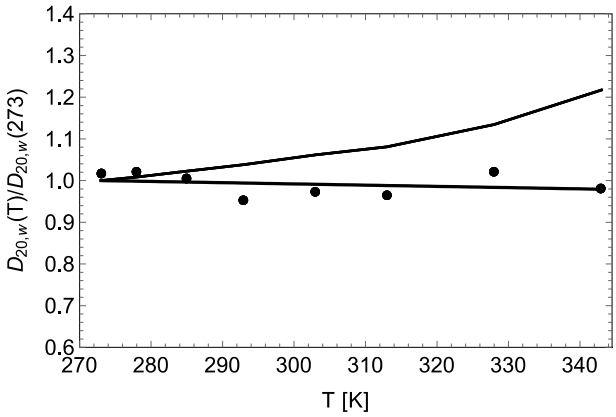

Fig. 1. Ratio of corrected diffusion coefficients, $D_{20,w}(T)/D_{20,w}(273)$, vs. temperature, *T*. The black disks are $D_{20,w}^{Exp}(T)/D_{20,w}^{line}(273)$ ratios computed from the experimental diffusion coefficients of WS and their best-fit straight line given by Eq.(1). The thick straight line is the best-fit ratio line, $D_{20,w}^{line}(T)/D_{20,w}^{line}(273)$ given by Eq.(2). The thin rising "curve" is the ratio, $D_{20,w}^{GKV}(T)/D_{20,w}^{GKV}(273)$ computed for the persistence lengths reported by GKV by using YF theory, as described in the text.

The ratios, $D_{20,w}^{Exp}(T)/D_{20,w}^{line}(273)$, are plotted along with the best-fit ratio line, $D_{20,w}^{line}(T)/D_{20,w}^{line}(273)$, and also the "curve" of $D_{20,w}^{GKV}(T)/D_{20,w}^{GKV}(273)$ vs. *T* in Fig. 1. The latter "curve" is obtained simply by connecting the discrete values with straight-line segments.

As anticipated, with increasing temperature the $D_{20,w}^{GKV}(T)/D_{20,w}^{GKV}(273)$ ratios lie increasingly farther above both the experimental $D_{20,w}^{Exp}(T)/D_{20,w}^{line}(273)$ ratios and the $D_{20,w}^{line}(T)/D_{20,w}^{line}(273)$ ratios, and obviously provide a rather poor match to the experimental data of WS. This discrepancy is quantified in the following ways.

The mean slope of the $D_{20,w}^{GKV}(T)/D_{20,w}^{GKV}(273)$ curve from 273 to the highest experimental temperature of GKV, namely 333 K, is $(D_{20,w}^{GKV}(333)/D_{20,w}^{GKV}(273) - 1)/(60) = 2.77 \times 10^{-3}\,\text{K}^{-1}$, which differs from mean slope of the best-fit ratio line by 6.1 standard deviations of the latter.

The ratio of the probability that the $D_{20,w}^{GKV}(T)/D_{20,w}^{GKV}(273)$ ratios give rise to the experimental D_T^{Exp}/D_{273}^{line} data of WS to the probability that the best-fit ratio line (bfrl) gives rise to those same data is given by,

$$\Pi_{GKV}/\Pi_{bfrl} = \exp[-\chi_{GVK}^2/2]/\exp[-\chi_{bfrl}^2/2] \quad (3)$$

Table 1
Table of experimental and predicted $D_{20,w}(T)$ values and ratios thereof for the 19,285 bp linear phage ϕ29 DNA (in ~110 mM univalent cations) at different temperatures. The P_{GKV} are taken from the curve of *P* vs. *T* in Fig. 7 of GKV, including a short linear extrapolation from 65 to 70 °C. The $D_{20,w}^{GKV}$ at each value of *T* is calculated by YF theory for the indicated value of P_{GKV} and a hydrodynamic diameter of 2.5 nm, and the relevant theoretical ratio, $D_{20,w}^{GKV}(T)/D_{20,w}^{GKV}(273)$, is reckoned directly. The $D_{20,w}^{line}(T)$ are calculated from the best-fit straight line through the experimental data of WS after correction of the latter to 20,w conditions, and the relevant theoretical ratios for the best-fit line, $D_{20,w}^{line}(T)/D_{20,w}^{line}(273)$, are reckoned directly. The $D_{20,w}^{exp}(T)$ are the measured values of WS after correction to 20,w conditions, and are divided by $D_{20,w}^{line}(273)$ to reckon the relevant experimental ratios.

T (K)	P_{GKV} (nm)	$D_{20,w}^{GKV}(T)/D_{20,w}^{GKV}(273)$	$D_{20,w}^{line}(T) \times 10^8$ (cm²/s)	$D_{20,w}^{line}(T)/D_{20,w}^{line}(273)$	$D_{20,w}^{Exp}(T) \times 10^8$ (cm²/s)	$D_{20,w}^{Exp}(T)/D_{20,w}^{line}(273)$
273	54.5	1.000	0.949	1.000	0.964	1.016
278	53.2	1.009	0.947	0.998	0.967	1.019
285	51.2	1.023	0.945	0.996	0.955	1.007
293	49.1	1.039	0.943	0.994	0.902	0.951
303	46.2	1.063	0.940	0.991	0.923	0.973
313	44.0	1.082	0.937	0.988	0.914	0.964
328	38.7	1.137	0.933	0.984	0.967	1.019
333	36.2	1.166	0.932	0.982	–	–
343	32.3	1.220	0.929	0.979	0.932	0.982

where the chi-squared values are given by,

$$\chi^2_{GVK} \equiv \sum_{i=1}^{8} (D^{GKV}_{20,w}(T_i)/D^{GkKV}_{20,w}(273) - D^{Exp}_{20,w}(T_i)/D^{line}_{20,w}(273))^2/\sigma_i^2 = 101.4 \quad (4)$$

$$\chi^2_{bfrl} \equiv \sum_{i=1}^{8} (D^{line}_{20,w}(T_i)/D^{line}_{20,w}(273) - D^{Exp}_{20,w}(T_i)/D^{line}_{20,w}(273))^2/\sigma_i^2 = 4.81 \quad (5)$$

where $\sigma_i = 0.030 \times 10^{-8}/0.949 \times 10^{-8} = 0.0316$ is the standard deviation of the ratio $D^{Exp}_{20,w}(T_i)/D^{line}_{20,w}(273)$, and the sums run over all temperatures *except* 333 K in Table 1. Inserting the results of Eqs.(4) and (5) into Eq.(3) yields finally the probability ratio, $\Pi_{GKV}/\Pi_{bfrl} = 1.06 \times 10^{-21}$. This value is unrealistically small, since it involves the assumption that the errors in $D^{Exp}_{20,w}(T)$ are distributed in Gaussian fashion so far into the wings of the distribution that such points would be rejected as experimental outliers, even if the distribution were actually Gaussian. Nevertheless, the probability that the $D^{GKV}_{20,w}(T_i)/D^{GKV}_{20,w}(273)$ ratios could account for the experimental $D^{Exp}_{20,w}(T_i)/D^{line}_{20,w}(273)$ ratios is so small that the $D^{GKV}_{20,w}(T_i)/D^{GKV}_{20,w}(273)$ ratios, and by inference the P_T/P_{273} ratios of GKV, are effectively ruled out *for the unstrained linear ϕ29 DNA*.

2.5. Tethered particle experiments

From measurements of tethered particle motions (TPM), Driessen et al. [40] obtained sufficiently steep mean negative slopes, $dP/dT < 0$, for DNAs of different composition over the range 296 to 345 K that the implied slope, $d\kappa_\beta/dT < 0$, was also significantly *negative* over that same range. However, a more recent study by Brunet et al. [41] using the same TPM method yielded a much smaller negative slope, $dP/dT < 0$, over the range from 288 to 338 K, which implied a mean slope, $d\kappa_\beta/dT \geq 0$, consistent with the majority of other studies. Examination of the data in their Fig. 4 indicates that over the more limited range from 288 to 323 K, the negative slope, dP/dT, is substantially smaller than that obtained over the full 288 to 338 K range, and implies a *significantly* positive value of $d\kappa_\beta/dT > 0$ over that more limited range. In addition, Brunet et al. plausibly demonstrated that the much steeper negative slope, $dP/dT < 0$, observed by Driessen et al. was an artifact due to blurring of the bead positions by time-averaging during the 20 ms exposure time used for each pixel, which significantly exceeds the relaxation time of the tether-bead system at the higher temperatures, where the viscosity is low and the tether-bead relaxation is correspondingly more rapid than at lower temperatures. After correcting for the bias introduced by such blurring in the data of Driessen et al., it was found that $d\kappa_\beta/dT \geq 0$ over the full range for those data as well. Thus, it now appears that, when properly corrected for time-averaging bias, the TPM studies of both Driessen et al. [40] and Brunet et al. [41] give mean values, $d\kappa_\beta/dT \geq 0$, over the full range, and $d\kappa_\beta/dT > 0$ over the more limited 288 to 323 K range, in agreement with the majority of other experiments.

2.6. Topoisomer distribution measurements and analyses

GKV[15] measured the relative populations of covalently closed circular topoisomers formed by ligation of nicked pUC19 DNAs (N = 2686 bp) at various temperatures from 278 to 333 K in buffers containing 39.9 or 37.2 mM univalent cations (after taking account of the Tris•H^+ fraction of the buffer) plus 10 mM Mg^{2+}.

Each topoisomer is subject to a Calugareanu, White, Fuller (CWF) constraint, $\Delta Lk = Wr + \Delta Tw$, wherein the linking difference, ΔLk, is the difference between the *integral* linking number of the covalently closed topoisomer and its non-integral intrinsic twist Tw_0, Wr is its writhe, and the twist difference, $\Delta Tw = Tw\text{-}Tw_0$, is the difference between the prevailing net twist and the intrinsic twist. DNA in the six most populous, and most accurately quantified, *equilibrium* topoisomers of a 2686 bp DNA is only very weakly strained. From the relative populations of such topoisomers, GKV ultimately obtained the T-dependent values of $(<Wr^2>_u + <\Delta Tw^2>_u)$ for the corresponding *unconstrained* DNA, which is denoted by the subscript u. That *unconstrained* DNA is a fictitious, geometrically and physically forbidden, covalently closed circular DNA, wherein the *linking number* is continuous and variable rather than an integral invariant, so the CFW constraint does not hold, and fluctuations in Wr and ΔTw occur independently, while at the same time all bending and torsion springs are assumed to remain intact.

The procedure used by GKV to obtain $(<Wr^2>_u + <\Delta Tw^2>_u)$ from the experimental data is puzzling, because the quantity obtained directly from the topoisomer distribution was actually their K (denoted as E_T in our lab), which is proportional to the torque constant for supercoiling. The analysis of GKV leading to $(<Wr^2>_u + <\Delta Tw^2>_u)$ involves assertions that are not strictly valid and the explicit or implicit use of three equations that are not rigorously correct, as detailed in the Supplementary Information S1. Nevertheless, their final result,

$$E_T = N/(2(<Wr^2>_u + <\Delta Tw^2>_u)) \quad (6)$$

is rigorously correct, whenever the relative probability distribution of Wr in the unconstrained DNA is Gaussian, as proved analytically in Appendix A of ref. 42. Analysis of their topoisomer distributions yielded the E_T values from 278 to 315 K in Table 2.

For an unconstrained DNA, $<\Delta Tw^2>_u$ is easily evaluated analytically for any *assumed* value of α by omitting all contributions of the bending springs and interduplex interactions to the total energy in the configuration integral. After subtracting the $<\Delta Tw^2>_u$ computed for the *assumed* value of α from the experimental value of $(<Wr^2>_u + <\Delta Tw^2>_u)$, one is left with a conditional experimental estimate of $<Wr^2>_u$.

For unconstrained DNAs, $<Wr^2>_u$ was reckoned via Monte Carlo simulations omitting all contributions of the torsion springs to the total energy (GKV). The value of P at each temperature was determined by trial and error using an analytical expression for $<Wr^2>_u$ that was parameterized to accurately represent simulated values for a wide selection of different lengths, effective hard cylinder diameters, d, and P-values c.f. Eqs.(2) and (3) of ref. 15. Of course, the value of P obtained at each temperature depends upon the α-value that was assumed in the calculation of $<\Delta Tw^2>_u$.

Table 2
Table of persistence lengths $P(T)$and bending elastic constants κ_β obtained from the measured $<\Delta Lk^2> = N/(2\ E_T)$ for topoisomers of pUC19 DNA (N = 2686 bp), when *measured* T-dependent torsion elastic constants $\alpha(T)$ (of an 1876 bp restriction fragment of pBR322 reported by DHS) are used instead of the constant T-independent value *assumed* by GKV.

T	$<\Delta Lk^2>$ (turn^2)	E_T (or K)	$\alpha(T)\times10^{19}$ (J)	$P(T)$[a] (nm)	$P(T)$[b] (nm)	κ_β[b] $\times10^{19}$ (J)
278	0.96	1399	8.59	53.4	51.1	5.81
293	1.025	1310	7.67	52.7	49.5	6.02
298	1.045	1285	7.37	52.8	49.3	6.13
303	1.065	1261	7.06	53.0	49.1	6.25
310	1.10	1221	6.63	53.1	48.6	6.39
315	1.13	1188	6.32	53.0	48.1	6.47
333	1.40	959	5.22	44.5	38.1	5.62
333	1.23[c]	1090[c]	5.22	55.1[c]	48.1[c]	7.09[c]

[a] These values are reckoned according to the protocol of GKV using $\alpha(T)$, h = 0.34 nm, and d = 5 nm, as described in the text.
[b] These values are reckoned according to the protocol of GKV using $\alpha(T)$, $h_{av}(T)$ (obtained from Eqs.(11) and (12) using h_0 = 0.325 nm), and d = 6 nm, as described in the text.
[c] These values are obtained by extrapolating the best-fit straight line of E_T vs. T over the range 278–315 K to 333 K, where the extrapolated value is E_T = 1090.

GKV *assumed* that the same *constant* value of the torsional rigidity, $C = 3.1 \times 10^{-28}$ J m, or equivalently $\alpha = 9.117 \times 10^{-19} \cong 9.12 \times 10^{-19}$ J (obtained using, $h = 0.34$ nm), applied to the six most weakly strained topoisomers of pUC19 DNA with $|\Delta Lk| \leq 3$, over a 55° range of temperatures from 278 to 333 K. The resulting *P*-values agreed quite well with those obtained from cyclization kinetics (CK) measurements of the *j*-factors of ~200 bp DNAs over the range of *T* where the two measurements overlapped [15]. However, this by no means proves that the persistence lengths and torsion elastic constants are actually the same in both the ~200 bp and 2686 bp species, for two reasons. First, there is a continuum of alternative pairs of α and P values that would yield precisely the same value of ($<Wr^2>_u + <\Delta Tw^2>_u$) for the 2686 bp topoisomers at any given temperature, and the assumption that α is independent of temperature is not only unjustified, but almost certainly incorrect, as detailed below. Second, it is highly doubtful that the CK experiment and data analysis protocol produces accurate *j*-factors over a wide range of temperatures, as noted below.

2.7. A previous study of the origin of the T-dependence of E_T

DHS [16] investigated the origins of the unexpectedly steep declines of the E_T (or K) values of large DNAs ($N > 3000$ bp) with increasing T that were manifested in (i) calorimetric measurements of the heat released upon supercoil relaxation at 310 K [43], and (ii) direct measurements of E_T for pBR322 DNA over the temperature range from 308 to 358 K [44]. In order to account for the substantially negative observed slopes (dE_T/dT), either the bending elastic constant κ_β or the torsion elastic constant α, or both, must decline significantly with increasing T. The problem is how to *independently* determine the value of α at each temperature.

Because twisting and bending motions take place on somewhat different time-scales, measurements of the twisting and bending dynamics over a sufficiently wide time span can in principle disentangle the torsion and bending elastic constants. The elastic constants sampled by *time-resolved fluorescence polarization anisotropy* (FPA) experiments are *fast relaxing* dynamic values, α_f and $\kappa_{\beta f}$, which govern Brownian twisting and flexure on their respective short time-scales, and must *equal* or *exceed* the long-time equilibrium values of those same elastic constants. Because there is presently no evidence that α_f significantly exceeds the long-time equilibrium value of α, the same symbol α will be used here for both values. However, the value of α obtained by FPA depends somewhat upon the *assumed* value of the *fast-relaxing* component of the bending elastic constant, $\kappa_{\beta f}$, or equivalently the *fast relaxing* persistence length, $P_f = h\kappa_{\beta f}/k_BT$, that applies during the 130 ns time span of that experiment [13,45]. (This fast-relaxing component was called the *dynamic* persistence length and denoted by P_d in previous reports from the author's lab. However, most of the DNA community now uses the symbol P_d to denote all relaxing components, regardless of whether they relax fast or slow.) The *slow relaxing* component (s) of the bending elastic constant encompasses all bends that relax on time-scales ≥10 μs, and its associated persistence length is denoted by P_s [45]. The apparent bending elastic constant associated with slow relaxing bends is given by, $\kappa_{\beta s} = (P_s/h)k_BT$. In general there are also *non-relaxing* (n) components that arise from intrinsic curvature associated with a particular sequence. That non-relaxing contribution to the persistence length is denoted by, P_n, and its apparent bending elastic constant by, $\kappa_{\beta n} = (P_n/h)k_BT$. This component is commonly regarded as an average over the sequence of a DNA.

Because the maximum time-span of the FPA experiment (130 ns) is short compared to the end-over-end rotational relaxation time of a 140 bp DNA, $(6D_R)^{-1}$–1000 ns, where D_R is the rotational diffusion coefficient of the DNA about a transverse axis, FPA measurements of α are largely insensitive to the *equilibrium* value of P for DNAs with $N \geq 140$ bp, although they remain somewhat sensitive to the *fast-relaxing* bending elastic constant, $\kappa_{\beta f}$.

The total persistence length is accurately related to the fast, slow, and non-relaxing components noted above by,

$$1/P_{tot} = 1/P_f + 1/P_s + 1/P_n \quad (7)$$

and the corresponding (apparent) bending elastic constant should be adequately approximated by [45],

$$1/\kappa_{\beta tot} = 1/\kappa_{\beta f} + 1/\kappa_{\beta s} + 1/\kappa_{\beta n} \quad (8)$$

The relation (7) with $1/P_d$ in place of $1/P_f + 1/P_s$ was shown to be remarkably accurate for several kinds of model filaments with different base-pair step parameters for both fluctuating dynamic (f and s) and non-relaxing (n) bends [11].

The distinction between fast and slow relaxing bends is irrelevant for equilibrium properties, but is almost certainly significant for understanding experiments where the rates of relaxation of the bends are important, such as FPA or cryoEM.

2.8. Experimental values of P_f and its variations with T and ionic conditions

For linear DNAs in solution at ~293 K, P_f equals or exceeds 150 nm, which in turn exceeds the corresponding equilibrium value (P~50 nm) by ~3-fold or more [45]. Relevant experiments leading to, or supporting, this originally unexpected result include: (1) decays of transient photo-induced dichroism (TPD) [46,47], and transient polarization grating (TPG) [45,48] signals in experiments on DNA:intercalated-methylene blue complexes, and experiments on DNA:intercalated-ethidium complexes with various lengths ≤72 bp [48]; (2) short-time transients due to bending in the off-field decays of the ED [31,34,49] and EB [50] of DNAs of various lengths [51–53]; and (3) epr linewidth (EPRLW) measurements of site-specifically spin-labeled DNAs with 14 to 100 bp [54]. These measurements were performed under different ionic conditions. Specifically, EPRLW measurements in ~ 110 mM univalent cations yielded, $P_f = 170 \pm 20$ nm; TPG measurements in 4 mM univalent cations yielded $P_f = 200\ (-20, +30)$ nm; and ED and EB measurements in ~1 to 2 mM univalent cations yielded, $200 \leq P_f \leq 220$ nm, all at or near 293 K. Evidently, most of the mean squared curvature of natural DNAs either relaxes on times scales longer than the ~10 μsec span of the TPG experiments or arises from non-relaxing bends. Combined FPA and TPG measurements captured the twisting, flexing, uniform azimuthal rotation, and uniform end-over-end tumbling of a 200 bp linear DNA in 4 mM univalent cations at 294 K, and enabled the simultaneous determination of $P_{tot} = 50$ nm, $P_f = 200\ (-20, +30)$ nm, and $\alpha = 5.54 \times 10^{-19}$ J [45]. A brief review of the relevant experiments and a fuller description of the TPG experiment are given elsewhere [45,48].

The variation of P_f with temperature was briefly addressed in two studies. (1) EPRLW measurements indicate no significant change in $\kappa_{\beta f}$ from 273 to 283 K [54]. (2) ED measurements on three fragments (138, 166, 179 bp) in ~110 mM Na^+ plus 10 mM Mg^{2+} provided longest *bending* relaxation times (much shorter than the terminal end-over-end rotational diffusion times), which after dividing out the viscosity indicated no *significant* change in $\kappa_{\beta f}$ with increasing T from 283 to 293 K [31,34,49]. Additional ED experiments on the 179 bp fragment in 2 mM Na^+ plus 0.2 mm EDTA plus 0.1 mM Mg^{2+}, yielded longest bending times that, after dividing out the viscosity, also indicated no *significant* change in $\kappa_{\beta f}$ over the much larger range from 275 to 313 K. Collectively, these observations suggest that any variation of $\kappa_{\beta f}$ with T over this latter T-range is rather slight.

Throughout the 1990s, when analyzing FPA data on DNAs in ~0.1 M ionic strength in the presence or absence of Mg^{2+} near 293 K, it was typically *assumed* in our laboratory that $P_f = 150$ nm, which is now known to be a modest underestimate in the absence of Mg^{2+}, and in turn leads to a modest *overestimate* of α under such conditions. In the absence of any systematic information regarding the effect of Mg^{2+} on P_f, it *assumed* here that: (1) $P_f = 150$ nm in the presence of ~40–100 mM univalent cations *plus* 5.5–10 mM Mg^{2+}; (2) $P_f = 170$ nm in 100–110 mM univalent cations; (3) $P_f = 180$ nm in ~35–50 mM

univalent cations; and (4) $P_f = 200$ nm in 2–5 mM univalent cations.

2.9. T-dependent torsion elastic constants measured by FPA

Typically, α-values were determined by fitting appropriate theory [13,55,56] with an assumed value, $P_f = \infty$, to the FPA data in order to extract the best-fit lower bound (LB) torsion elastic constant, α_{LB}, and then multiplying that by a correction factor, $\alpha_{actual}/\alpha_{LB}$, to obtain the actual value that would have been found by using the prevailing value of P_f instead of ∞ [13,57]. Such correction factors are given by a previously published "universal" curve of $\alpha_{actual}/\alpha_{LB}$ vs. $1/P_f$ [57]. That curve was obtained by first simulating FPA data for a range of α-values and a range of P_f values (from 50 nm to ∞) for each α-value, and then fitting such simulated data using $P_f = \infty$ [57]. The resulting correction factors are practically independent of the input value of α_{actual} and are, respectively, $\alpha_{actual}/\alpha_{LB} = 1.35$, 1.30, 1.28, and 1.26 for, respectively, $P_f = 150$, 170, 180, 200 nm.

DHS measured α for an 1876 bp linear restriction fragment of pBR322 in three different buffers, extracted best-fit values of α by assuming a constant value, $P_f = 150$ nm, for which $\alpha_{actual}/\alpha_{LB} = 1.35$. In each case they found a substantial decline in α with increasing T from 278 to 333 K with a similar slope in each buffer (c.f. Fig. 3 ref.16). Similar declines also were observed for a 1764 bp fragment of p30δ DNA, and a linear 7229 bp M13mp8 DNA [27]. The best-fit straight line through the α-values obtained using, $\alpha_{actual}/\alpha_{LB} = 1.35$, for the 1876 bp DNA in ~39 mM univalent cations plus 5.5 mM Mg^{2+} is given by,

$$\alpha\,(T) = (8.9–(0.0614)(T - 273))\ \text{x}10^{-19}\ \text{J} \quad (9)$$

The α-value at each of several temperatures spanning the range studied by GKV is reckoned via Eq.(9), and the resulting values are listed in Table 2.

The following relations summarize results of FPA experiments on linearized unstrained bacterial plasmids and their subfragments under other ionic conditions.

For ~100–110 mM univalent cations, $P_f = 170$ nm,

$$\alpha\,(T) = ((6.1 \pm 0.4)–(0.0671)(T - 293))\ \text{x}10^{-19}\ \text{J} \quad (10a)$$

For ~ 35–50 mM univalent cations, $P_f = 180$ nm,

$$\alpha\,(T) = ((6.2 \pm 0.4)–(0.0671)(T - 293))\ \text{x}10^{-19}\ \text{J} \quad (10b)$$

Eq.(10a-b) reflect measurements on many different plasmid DNA samples under the indicated ionic conditions at ~293 K. Hence, the reference temperature is shifted from 273 K in Eq.(9) to the 293 K in Eq. (10a-10b). Eq.(10a-10b) incorporate the approximate slopes with temperature that were measured for just three different DNAs, only one of which was studied under three different ionic conditions.

As a cautionary note, certain linear *viral* DNAs, such as ϕ29, λ, and M13mp7, at 293 K exhibit significantly (~0.80)) lower values, $\alpha = (4.9 \pm 0.4)\text{x}10^{-19}$ J in ~10 mM univalent cations [13,57]. In ~100 mM univalent cations, ϕ29 exhibits an even lower value, $\alpha = (4.55 \pm 0.4)\text{x}10^{-19}$ J [13,57], which remains constant over the T-range from 283 to 333 K [80]. These findings, which do not pertain to plasmid DNAs, are addressed in section (4) below.

2.10. Summary of the two-state cooperative transition model

At every position in the sequence, the states a and b are involved in a cooperative equilibrium, $a \Leftrightarrow b$, which is characterized by an equilibrium constant, B, for an isolated base-pair, and a cooperativity parameter, J, that reflects the free energetic cost of unlike (ab or ba) neighbors relative to that for like (aa or bb) neighbors. The model yields an expression for the fraction, f_b, of all bp in the b state in terms of B and J (c.f. Eq.(15) below) [1]. From f_b, the average values of h, $1/\alpha$, and $1/\kappa_\beta$ for the entire molecule are simply reckoned. Fitting the model to relative extension vs. force data for an untwisted DNA (ref [1] & Mosconi) indicated that B is very close to 1.0, even in the presence of forces up to 3.9 pN, and that, $J \leq 4.4855 \times 10^{-3}$, so unlike neighbors, or junctions between different secondary structures, are scarce. At the midpoint of the transition, the average size of a domain of a or b is, $1 + 1/J \geq 224$ bp (large cooperativity). The close proximity of B to 1.0 indicates that the difference in free energy per bp between the a and b states is very small compared to k_BT, and this circumstance prevails even in the presence of tensions up to several pN, or variations in T from 278 to 315 K, or addition of Mg^{2+} from 0 to 10 mM in moderate univalent cation concentration. However, the large cooperativity associated with the very small J enables the small changes in B due to such small perturbations to significantly shift the value of f_b. The original study yielded three sets of best-fit values of the four parameters, $\delta = h_b - h_a$, J, α_a, and α_b, spanning the statistically acceptable range [1].

2.11. Revision of α_a and α_b for parameter set 3

The appearance of three new magnetic tweezers measurements [14] of the torsional rigidity of a single DNA under tension necessitated a redetermination of the best-fit values of α_a and α_b for parameter set 3. This is described in Supporting Information S2. The new optimal values are: $\alpha_a = 4.44 \times 10^{-19}$ J, and $\alpha_b = 12.32 \times 10^{-19}$ J, which are listed in Table 3 below.

2.12. Analysis of topoisomer distribution data of GKV using measured T-dependent torsion elastic constants

Experimental values of $(<Wr^2>_u + <\Delta Tw^2>_u)$ were designated as $<(\Delta Lk)^2>$ by GKV[15] and plotted vs. T in their Fig. 5. From the smooth curve of GKV through those data, values of $(<Wr^2>_u + <\Delta Tw^2>_u)$ at various temperatures were extracted, and are listed as $<(\Delta Lk)^2>$ in Table 2. Also listed in Table 2 are the corresponding values of E_T, reckoned according to Eq.(6). The value of $<\Delta Tw^2>_u = Nk_BT/(\alpha(T)\cdot(2\pi)^2)$ is readily calculated at each temperature and subtracted from $<(\Delta Lk)^2> = (<Wr^2>_u + <\Delta Tw^2>_u)$ to obtain the corresponding value of $<Wr^2>_u$. The equilibrium persistence length P required to yield the same value of $<Wr^2>_u$ is determined by trial and error using Eqs.(2) and (3) of GKV [15], initially with the same effective hard-cylinder diameter, $d = 5.0$ nm, and rise per bp, $h_0 = 0.34$ nm, used by those authors. The resulting values obtained for the equilibrium persistence length P at each temperature are listed under $P(T)^I$ in Table 2. This protocol is identical to that of GKV, except that independently *measured* T-dependent values of $\alpha(T)$ were employed instead of the T-invariant value, $\alpha = 9.12 \times 10^{-19}$ J, *assumed* by GKV. From 278 to 315 K the equilibrium persistence lengths obtained using these T-dependent α-values all lie in the range, $P = 53.1 \pm 0.3$ nm, which implies no significant variation of P with T over that range. However, between 315 and 333 K, P apparently declines to 44.5 nm, about 0.84 times its nearly constant value over the range, 278 to 315 K.

When the E_T values in Table 2 are plotted vs. T (not shown), they follow closely a descending straight line with best-fit slope, $dE_T/dT = -5.60 \pm 1.0\,\text{K}^{-1}$, from 278 K to 315 K, before falling more steeply from 1188 at 315 K to 959 at 333 K. If the straight-line portion of the curve were extended from 315 to 333 K, it would take the value, $E_T = 1090$, at 333 K, which is also listed in Table 2. That higher E_T value in turn would yield, $P = 55.1$ nm, also listed under $P(T)^I$ in Table 2, which is close to the range of the other P values. This raises the possibility that the experimental value of E_T at 333 K, which is an average of two significantly different values, is anomalously low for some reason, possibly involving DNA aggregation, as discussed subsequently.

A second analysis of the GKV data was performed in the following way. The value of $<\Delta Tw^2>_u$ at each T is reckoned from $\alpha(T)$, and subtracted from $<(\Delta Lk)^2>$ to obtain the corresponding value of $<Wr^2>_u$, as in the first analysis above. Then the $\alpha_a = 4.44 \times 10^{-19}$ J and

Table 3
Fixed parameters of the cooperative two-state model employed in this work. The quantities, δ and J, were taken from parameter set 3 of Table 2 in ref. 1. This value of δ is close to the 0.05 nm estimated by Zettl et al. [5] from X-ray scattering studies of short DNAs labeled with gold colloids. The value of h_0 yields, h_{av} = 0.325 nm, for an unstrained DNA in 0.1 M NaCl at 293 K, close to the value, 0.323 ± 0.01 nm, determined by Zettl et al. [5] for short DNAs under such conditions.

δ (nm)	h_0 (nm)	J	α_a (J)	α_b (J)	$\kappa_{\beta a}$ (J)	$\kappa_{\beta b}$ (J)
0.0487	0.325	4.4855×10^{-3}	4.44×10^{-19}	12.32×10^{-19}	8.00×10^{-19}	5.35×10^{-19}

$\alpha_b = 12.32 \times 10^{-19}$ J of parameter set 3 of the two-state model are used in the relation [1,2],

$$1/\alpha(T) = (1 - f_b(T))/\alpha_a + f_b(T)/\alpha_b \quad (11)$$

to reckon the fraction, $f_b(T)$, of bp in the longer b state at each temperature from the corresponding measured $\alpha(T)$ values in Table 2. That in turn is used to compute the average rise per bp at each temperature according to [1],

$$h_{av}(T) = h_0 - \delta/2 + f_b \cdot \delta \quad (12)$$

where δ = 0.0487 nm is the difference in length between the b and a states for parameter set 3, and h_0 = 0.325 nm is a constant chosen to yield $h_{av}(T)$ = 0.325 nm in the absence of force (in ~100 mM NaCl at 293 K), which lies near the center of the range, 0.323 ± 0.01 nm, measured by X-ray scattering for 10 to 35 bp DNAs labeled by gold colloids under the same conditions [5]. The $P(T)^{II}$ value required to yield the known value of $< Wr^2 >_u$ is then determined by trial and error using Eqs.(2) and (3) of GKV with the appropriate value of $h_{av}(T)$ and the effective hard-cylinder diameter, d = 6.0 nm. This protocol differs from that of GKV by the use of $\alpha(T)$ and $h_{av}(T)$ instead of the constant values assumed by GKV, and by the use of an effective hard-cylinder diameter, d = 6.0 nm instead of the 5.0 nm used by GKV. These $P(T)^{II}$-values are also listed in Table 2. They are somewhat smaller than the corresponding $P(T)^{I}$-values and decline slightly from 278 to 315 K.

The values of $P(T)^{II}$ depend slightly on the choice of effective hard-cylinder diameter. The value, d = 5.0 nm, used by GKV was estimated from measurements of knotting probabilities under various solution conditions, and comparison with relevant theory [58]. Because no measurements were made for the particular mixed electrolyte conditions (~38 mM univalent cations plus 10 mM Mg^{2+}) used in the experiments of GKV, some interpolation is required, which admits significant uncertainty in d. Traditionally, d was taken to be the effective hard cylinder diameter that yields the same second virial coefficient as the non-linear Poisson-Boltzmann (NLPB) potential calculated for a 24 Å diameter uniformly charged cylinder with either 100% or 73% of the full DNA charge. In the present study, the value of d was reckoned for a buffer containing 38 mM univalent cations plus 10 mM Mg^{2+} (plus all necessary univalent anions to attain electroneutrality). (After accounting for the fractions of the total Tris that are present as $TrisH^+$ and Tris at the stated pH 7.6 at 298 K using the known pK_a = 8.06, the Taq Ligase Buffer used by GKV was found to contain 39.9 mM univalent cations plus 10 mM $MgCl_2$, and their T4 Ligase Buffer was found to contain 37.2 univalent cations plus 10 mM $MgCl_2$, both of which are close to 38 mM univalent cations plus 10 mM Mg^{2+}.) The series method used to calculate the reduced NLPB potential was described in the book by Rice and Nagasawa [59], and was briefly outlined in the Appendix A of ref. [60]. The values calculated for the conditions noted above were, d = 6.2 nm, for 100% of the full DNA charge and, d = 6.0 nm, for 73% of the full charge. The value, d = 6.0 nm, was used to reckon the P^{II} and $\kappa_\beta{}^{II}$ values in Table 2.

When the value d = 5.0 nm was used, the $P(T)^{II}$-values obtained were larger than those reckoned using d = 6.0 nm by ≤1.9 nm at all $T \leq$ 315 nm. In both cases (i.e. d = 6.0 and d = 5.0 nm), the relative *increase* in $\kappa_\beta{}^{II}$ with increasing T was ~1.11- fold over the range 278 to 315 K.

2.13. A plausible explanation for the anomalously low value of P at 333 K

DHS routinely examined each sample at every temperature by DLS in order to detect any possible aggregation, especially in the buffer containing 5.5 mM Mg^{2+} ions plus ~45 mM univalent cations. They reported evidence of significant aggregation of DNA in that buffer at 333 K, but *not* in that same buffer at lower temperatures, and *not* in solutions without Mg^{2+} at any temperature up to 333 K [16,27]. No value of α was reported for the single condition (among all of those studied), where aggregation was observed.

The aggregation at 333 K in the presence of 5.5 mM Mg^{2+} plus 45 mM univalent cations is likely related to the decline in the relative dielectric constant of water from 85.8 to 66.8 as T rises from 278 to 333 K. A DNA that did not condense in 20 mM Mg^{2+} plus ~5 mM univalent cations in water at 293 K, spontaneously condensed to form hexagonal arrays in a solution with the same ionic concentrations in a 30 *v*/v % mixture of methanol and water at the same temperature, which has a relative dielectric constant of 64.9 [61]. Hence, it is plausible that the 333 K samples of GKV, which contained 10 mM Mg^{2+} in ~38 mM univalent cations, also exhibited significant aggregation at 333 K. Without evidence to rule out aggregation, the results of GKV at 333 K are equivocal.

What effect might interduplex attractions responsible for such aggregation have on E_T? Effective interduplex attractions induced by osmotic exclusion forces were previously shown to diminish E_T of pUC18 DNA (2686 bp) linearly with increasing concentration of polyethylene glycol (PEG 8000) down to 0.53-fold in 7.5 (*w/v*) % PEG [62]. It is plausible that Mg^{2+}-induced interduplex attractive forces in the 333 K samples of GKV might also significantly diminish E_T, which would lead to an anomalously low value of apparent P in that solution. Thus, it remains a possibility that, for the unaggregated DNA, $P(T)^{II} \cong$ 48.8 nm, even at 333 K. If so, the near invariance of P^{II} to increasing T from 278 to 333 K would be similar to that of ϕ29 DNA [37].

2.14. Experimental evidence for the assumptions of GKV and DHS regarding α

The very different assumptions made by DHS and GKV regarding the value of α and its variation with T lead to a large difference in conclusion regarding the T-dependence of the κ_β of weakly strained 2686 bp circular DNA. Hence, it is necessary to examine the experimental support for those two different assumptions.

Historically, many DNA scientists *supposed* that a given duplex sequence underwent only small fluctuations about a unique unperturbed conformation, whose α was a robust quantity, independent of moderate bending strains in ~200 bp circles, moderate tensions in single molecule pulling experiments, moderate variations of temperature, or the presence or absence of significant Mg^{2+} in the solution. GKV *assumed* that under all such more or less "normal" conditions the prevailing values would lie in the range, α = (9.1 to 9.5) x 10^{-19} J, which had been obtained by two different analyses [63,64] of a single set of topoisomer ratios for three circular DNAs of largely common sequence with 205, 207, and 217 bp in ~31 mM univalent cations plus 10 mM Mg^{2+} at 310 K (HW) [65]. However, extrapolation of this result to free unstrained linear DNA or to weakly strained large circular DNAs with low superhelix density has no *direct* experimental support

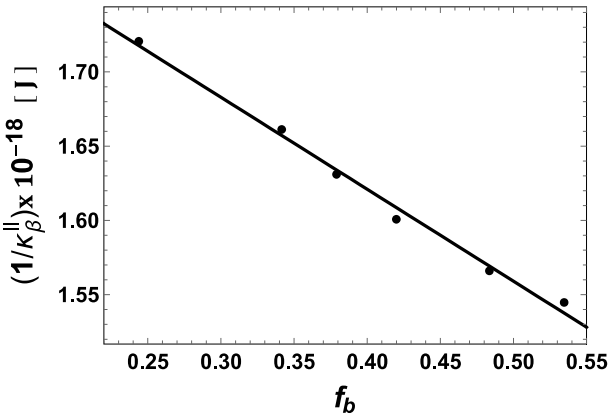

Fig. 2. Inverse bending elastic constant $1/\kappa_\beta^{II}$ vs. fraction of bp in the *b* state $f_b(T)$. The straight line is the best-fit of $1/\kappa_\beta^{II}$ by Eq.(13) with $\kappa_{\beta a}$ and $\kappa_{\beta b}$ as adjustable parameters. The data points correspond to $1/\kappa_\beta^{II}$ values from the last column in Table 2, which applies for an effective hard cylinder diameter, $d = 6$ nm. Values of $f_b(T)$ at each temperature were obtained from the measured values of $\alpha(T)$, by using Eq.11 together with $\alpha_a = 4.44 \times 10^{-19}$ and $\alpha_b = 12.32 \times 10^{-19}$ J from the parameter set 3 of the two-state cooperative model in Table 3. Best-fit bending elastic constants are: $\kappa_{\beta a} = 8.00 \times 10^{-19}$ J and $\kappa_{\beta b} = 5.35 \times 10^{-19}$ J.

whatsoever, and relies entirely on the aforementioned *supposition*. In fact, many studies preceding, and also subsequent to, that of GKV strongly contradict any notion that the unperturbed structure is unique or that there exists a robust and universally applicable value of α. Those studies are briefly described in Supporting Information S3, to which readers are referred.

The results in subsections (1)–(10) of S3 all either flatly contradict or seriously undermine any assumption that DNA exhibits a unique unperturbed conformation with a single robust and universally applicable value of α (as opposed to two or more coexisting conformations with different values of both α and κ_β). The *assumed* *T*-invariant value, $\alpha = 9.12 \times 10^{-19}$ J, that was adopted by GKV is therefore eschewed here in favor of the *measured* values listed in Table 2. As a consequence, the values of *P* for the 6 least strained topoisomers of the pUC19 DNA remain almost constant from 278 to 315 K, as indicated also in Table 2. The *T*-invariance or very weak *T*-dependence of these $P(T)^I$- and $P(T)^{II}$-values, and the implied increase in the corresponding κ_β^{II}-values with increasing *T* agrees well with the already noted increases of κ_β with *T* for many other DNAs.

3. Coupled variations in α and κ_β with temperature and other properties of the cooperative two-state model

3.1. Variations of $1/\alpha$ and $1/\kappa_\beta$ with T are linearly anti-correlated

The seemingly counterintuitive rise in κ_β with increasing *T* might be a consequence of simply shifting population from the *b* state (with the longer $h_b = h_0 + \delta/2$ and greater α_b) to the *a* state (with shorter $h_a = h_0 - \delta/2$ and lower α_a) of the two-state cooperative model, provided that $\kappa_{\beta a}$ exceeds $\kappa_{\beta b}$. To investigate this possibility, it is tentatively assumed that the intrinsic values α_a, α_b, $\kappa_{\beta a}$, and $\kappa_{\beta b}$ of the *a* and *b* states remain constant, independent of *T*, over the limited range from 278 to 315 K, so the entire change in α or κ_β is ascribed to a shift in population between the *a* and *b* states. The fraction $f_b(T)$ of sequence in the *b* state at each temperature in Table 2 is reckoned from the experimental values of $\alpha(T)$ in Table 2 by Eq.(11) with the α_a and α_b values from the model parameter set 3, which are given in the sentence preceding Eq.11 and in Table 3 below. By design, the experimental values of $1/\alpha(T)$ extracted from Table 2 are perfectly linearly correlated with $f_b(T)$. The bending elastic constants, $\kappa_{\beta a}$ and $\kappa_{\beta b}$, of the *a* and *b* states were estimated by least-squares fitting the linear relation,

$$1/\kappa_\beta = (1 - f_b(T))/\kappa_{\beta a} + f_b(T)/\kappa_{\beta b} \quad (13)$$

to the κ_β^{II} values in Table 2. Fig. 2 indicates how well the "experimental" κ_β^{II} data are fitted by Eq.13 with the best-fit values, $\kappa_{\beta a} = 8.00 \times 10^{-19}$ and $\kappa_{\beta b} = 5.35 \times 10^{-19}$ J over the range from 278 to 315 K.

The linear correlation of $1/\kappa_\beta^{II}$ with $f_b(T)$, is rather good. The implied linear correlation of $1/\kappa_\beta^{II}$ with $1/\alpha$ given is given in the Table of Contents graphic (shown in the abstract). This is consistent with a *T*-induced shift in the equilibrium position of a two-state model, wherein the *a* and *b* states exhibit *T*-invariant values of α_a and $\kappa_{\beta a}$, and α_b and $\kappa_{\beta b}$, respectively. The best-fit values, $\kappa_{\beta a} = 8.00 \times 10^{-19}$ J and $\kappa_{\beta b} = 5.35 \times 10^{-19}$ J, are listed along with other previously determined constants of the two-state model in Table 3. Under the present interpretation, increasing *T* shifts the $a \Leftrightarrow b$ equilibrium from the (longer, torsionally stiffer, flexurally softer) *b* state toward the (shorter, torsionally softer, flexurally stiffer) *a* state.

The present two-state model with constant values of α_a, $\kappa_{\beta a}$ and α_b, $\kappa_{\beta b}$ accounts for the observed variations of α and/or κ_β in response to: (1) externally applied tension [1], (2) bending-induced axial tension [2], (3) changes in temperature, and (4) the presence or absence of 5.5 mM Mg^{2+} ions in the presence of univalent cations over a limited range of concentrations. It actually affirms the widespread intuitive belief that the elastic properties of a *single* solid-like structure should be insensitive to such modest perturbations. The apparent contradictions of that belief are resolved by the coexistence of t*wo* different structures in equilibrium with one another, an equilibrium that is sensitive to modest changes in environmental parameters.

3.2. Variation of intrinsic linking number per bp with F and T

For two different DNAs, the intrinsic linking number (number of turns of one strand around the other) per bp actually increased linearly, albeit very modestly, with increasing tension up to 19 pN [66]. Moreover, the observed increase in the low force regime, $F \leq 3.0$ pN, is so slight that it does not differ significantly from zero for tensions ≤ 1.3 pN, and even at ~3.0 pN amounts to $\leq 0.05\%$ of the intrinsic linking number per bp in the absence of force, equivalent to a superhelix density, $\sigma \leq 0.0005$ [66]. No decline in slope toward a plateau at forces above 1.3 pN was detected, unlike the gradual saturation of the rise per bp and torsion elastic constant with increasing force above 0.74 pN, which characterize the two-state transition [1]. Subsequent data of Mosconi et al. [6] under similar conditions revealed no significant variation of the zero rotation (or equivalently zero superhelix density) position with increasing force from 0.13 pN to 0.91 pN, in agreement with ref. [66]. The fraction of bp in the *b* state climbs from ~0.46 at zero force to ~0.98 at 3.0 pN, yet that change is associated with only a negligibly small increase in intrinsic linking number per bp under the prevailing conditions (~120 mM univalent cations at 296 K) [66]. Apparently the increase in the rise per bp during the $a \Leftrightarrow b$ transition is accompanied by a negligibly small change in intrinsic linking number per bp, suggesting that the intrinsic linking numbers per bp of the *a* and *b* states are very similar, despite their distinctly different rises per bp and elastic constants. The very small twist-stretch coupling constant inferred from measurements at forces, $F \geq 1.3$ pN, which encompasses all extant measurements of that quantity [66,67], evidently pertains primarily to the *b*-state, which predominates in the range of forces sampled.

Upon increasing temperature *T* in the range 273 to 299 K, the intrinsic linking number per bp (φ) of large (5300–9850 bp) circular DNAs decreased linearly with a slope, $d\varphi/dT = -3.389 \times 10^{-5}$ turn $bp^{-1}\,K^{-1}$, under the prevailing ionic conditions (2 mM Mg^{2+}, 10 mM Tris HCl pH 8.0, 1 mM Na_3EDTA) [68]. A slightly smaller slope, $d\varphi/dT = -3.14 \times 10^{-5}$ turn $bp^{-1}\,K^{-1}$ was observed for a 2200 bp plasmid DNA, under the same ionic conditions [68]. These changes

agree well with the, $d\varphi/dT = -3.19 \times 10^{-5}$ turn $bp^{-1}\,K^{-1}$, measured by GKV over the 278–315 K range for small (~200 bp) circular DNAs in ~40 mM univalent cations plus 10 mM Mg^{2+}, despite a much greater fraction of bp in the *b* state in that case. Measurements on single DNAs under various tensions (0.3, 0.5, 0.7, 0.8, and 0.9 pN) at several temperatures in the range, 296 to 315 K, yielded similar slopes, $d\varphi/dT = -3.19 \times 10^{-5}$ and -2.92×10^{-5} turn $bp^{-1}\,K^{-1}$ for, respectively, 20.6 kbp and 7.9 kb constructs in ~160 mM univalent cations [69]. These slopes were largely independent of the applied force, although a marginally significant trend toward slightly increased magnitudes of $d\varphi/dT$ was detected at 0.8 and 0.9 pN.

Observations in the two preceding paragraphs suggest that intrinsic linking numbers per bp of the *a* and *b* states are not only very similar at 298 K, but also undergo similar variations with both tension and temperature. This raises a new question of how a transition between two states of different length and elastic constants could occur in such a way that the intrinsic linking number per bp changes only very slightly. That is a topic for future work.

3.3. Other values of dE_T/dT

The model parameters $\kappa_{\beta a}$ and $\kappa_{\beta b}$ were determined from the κ_β^{II} values in Table 2, which followed in large part from the E_T vs. T data of GKV. Three other extant measurements of E_T vs. T data gave discordant results for the slope, dE_T/dT. This matter is discussed in detail in S4 of Supplementary Information. Two of those other measurements were performed under rather low ionic strength conditions. Simulations of a 4349 bp DNA under such low ionic strength conditions using a realistic electrostatic interduplex potential revealed that the supercoiling free energy rises more rapidly than quadratically with ΔLk, such that the E_T determined under the assumption of quadratic behavior increases linearly with ΔLk [70]. After applying appropriate corrections, the slopes of those other two measurements *at constant* ΔLk lie within experimental error of the value, $dE_T/dT = 5.6 \pm 1.0$, obtained above (c.f. section 2.12.) for the data of GKV. The third extant slope is much larger and remains an outlier for unknown reasons.

4. Tests of the extended two-state cooperative transition model

The parameters in Table 3, except for $\kappa_{\beta a}$ and $\kappa_{\beta b}$, were determined by fitting the two-state model to data that were derived from experimental data by invoking *assumed* values of certain quantities, for example $P = 50$ nm, and also $h_{av} = 0.338$ nm, in the estimation of experimental α-values. It is now necessary to verify that the present more elaborate two-state model with non-constant values of κ_β and h_{av} is able to satisfactorily match directly the primary experimental data from single molecule pulling experiments of Mosconi et al. [6] without invoking any assumed values of P or h.

4.1. z_F/z_{max} vs. F

The two-state cooperative model with parameters, δ, h_0, and J, from Table 3 plus the previously determined equilibrium constant, $B_0 = 0.999283$, for the $a \Leftrightarrow b$ transition of an isolated bp under the prevailing conditions in the absence of force is used to calculate self-consistently at each force F the values of $f_b(F)$, $P(F)$, $h_{av}(F)$, and relative extension z_F/L_F in the direction of the applied force. The relative extension is given to high accuracy for all forces, $F \geq 0.25$ pN, and to acceptable accuracy down to $F = 0.18$ pN by the relative extension formula of Moroz and Nelson (MN) [71,72],

$$z_F/L_F = (1 - (0.5)/(P(F)\cdot F/k_B T - 1/32)^{0.5}) \quad (14)$$

where $L_F = N\,h_{av}(F)$ is the contour length in the presence of the pulling force, F. The present calculation begins with the equation,

$$f_{b0} = (0.5)\,(1-(B_0-1)/(((B_0 - 1)^2 + 4\cdot B_0\cdot J^2)^{0.5})) \quad (15)$$

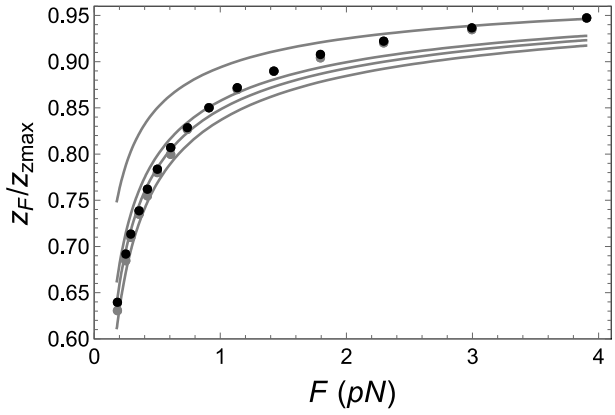

Fig. 3. Relative extension, z_F/z_{max}, vs. pulling force F for an untwisted DNA. Black disks are theoretical values predicted by the two-state model with the parameters in Table 3, and gray disks are experimental values of Mosconi et al. [6] The theoretical values were computed for the two-state model by assuming that, $z_{max} = (0.975)L_{max}$. Where gray experimental points are not visible, they are covered by black theoretical points. The continuous gray curves were computed for *inextensible* WLC models with different values of P. From top to bottom, the gray curves correspond to $P = 90$, 50, 44, and 38 nm. The curve for 44 nm has the smallest chi-squared value of any of the gray curves.

which is the principal result of the two-state model *in the absence of force* [1]. In the presence of an externally applied force, a similar equation applies, wherein f_{b0} is replaced by $f_b(F)$ and B_0 is replaced by,

$$B(F) = B_0\ \exp[+F\ \delta\ (z_F/L_F)/k_B T] \quad (16)$$

The z_F/L_F ratio in the exponent provides the mean projection of the pulling force onto the axis of the DNA, and can be expressed in terms of F, T, and $P(F)$ via Eq.(14). In the presence of a force, the mean rise per bp, $h_{av}(F)$, is given by Eq.(12), with $f_b = f_b(F)$, and the persistence length is given by, $P(F) = h_{av}(F)\kappa_\beta/k_B T$, where κ_β is expressed in terms of $f_b(F)$ via Eq.(13) with $f_b(F)$ in place of $f_b(T)$. All factors on the rhs of the *modified* Eq.(15) are expressed in terms of the known force, F, constants of the model, and the unknown $f_b(F)$, so it can be solved for $f_b(F)$ using the Mathematica NestList, FixedPoint, and/or NSolve commands, all of which yield the same results, although NSolve occasionally fails to yield a result. With $f_b(F)$ in hand, all of the relevant quantities can be calculated for a given F under the prevailing conditions (~0.1 M NaCl at 293 K) via Eqs.12–16.

The experimental data were presented as, z_F/z_{max}, where z_{max} is an unstated maximal extension, which was presumably determined by fitting an inextensible wormlike coil (WLC) model to the extension vs. force data over a range of forces with z_{max} and P as adjustable parameters. In view of Eq.(14), one can write, $z_F/z_{max} = (L_F/z_{max})(z_F/L_F)$, which gives,

$$z_F/z_{max} = (L_F/z_{max})(1 - (0.5)/(P(F)\cdot F/k_B T - 1/32)^{0.5}) \quad (17)$$

The value, $z_{max} = (0.975)(L_{max})$, where $L_{max} = N(0.325 + 0.0487/2) = N(0.349)$ nm is the largest possible value of L_F attainable by the model, was adopted, so that the theoretical value, $z_{3.9}/z_{max} = 0.947$, precisely matches the corresponding experimental value reported by Mosconi et al. for $F = 3.9$ pN. It is entirely likely that z_{max} was found to be slightly smaller than L_{max}, because it was determined by fitting an inextensible WLC model to experimental data for an *extensible* DNA over a range of forces, where the fraction of bp in the longer *b*-state was significantly <1.0 over the lower part of that range. Theoretical values of z_F/z_{max} (reckoned using $z_{max} = (0.975)\ L_{max}$) are compared with the corresponding experimental values reported by Mosconi et al. [6] in Fig. 3.

As noted above, z_{max} was obtained by fitting an inextensible WLC model to the experimental z-values by optimizing the values of z_{max} and P. Hence, no further adjustment should be applied to the WLC curves in

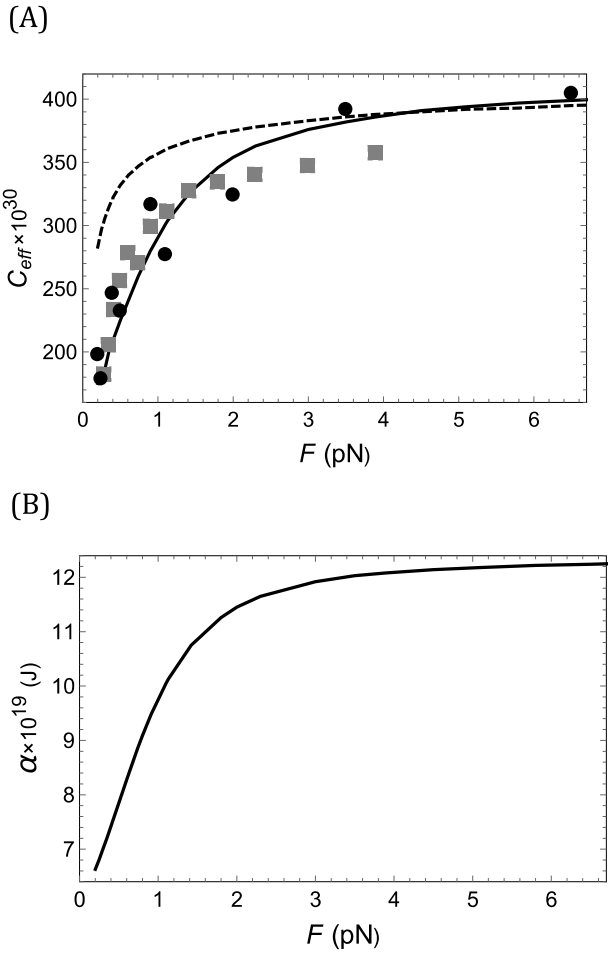

Fig. 4. (A) Effective torsional rigidity, C_{eff}, vs. force, F, for a single weakly twisted DNA molecule held at force, F. Thick black curve represents the theoretical values computed using the two-state model beginning with Eq. 10a and parameters given in Table 3 at $T = 293$ K, as described in the main text. The gray squares are experimental C_{eff} data of Mosconi et al. [6] and the black disks are from two different magnetic torque tweezers experiments of Lipfert and coworkers [7,14]. The dashed black curve is computed for an inextensible twisted wormlike coil (TWLC) with $P = 50$ nm, a rise per bp, $h = 0.34$ nm, and the maximum intrinsic torsion elastic constant of the two-state model, namely $\alpha = 12.32 \times 10^{-19}$ J m. (B) Intrinsic torsion elastic constant, α, of the effective springs between base-pairs vs. force, F, for the same DNA as in (A). The curve is computed using the two-state model beginning with Eq.(10a) and parameters given in Table 3 at 293 K. At zero applied force, $\alpha = 6.1 \times 10^{-19}$ J.

Fig. 3, because if one of them has the optimum P value, then it also will have the optimum z_{max}. The minimum value of chi-squared for the WLC occurs for $P = 44$ nm, but the chi-squared basin is relatively broad, climbing to about twice the minimum value at $P = 38$ and 50 nm.

Agreement between the two-state model and experiment is rather good, especially in view of the absence of adjustable parameters, apart from the minor adjustment of the unknown z_{max} to lie slightly below L_{max}. The visible differences between the two-state model predictions and experimental z_F/z_{max} ratios, which amount to relative errors of $\leq 0.9\%$ for all $F \geq 0.25$ pN, are probably less than the relative uncertainties in the experimental z_F/z_{max} ratios. The ratio, $h_{av}(3.9\text{ pN})/h_{av}(0.18\text{ pN}) = 1.066$, computed via Eq.(12) indicates a 1.066-fold increase in rise per bp and contour length upon increasing the force from 0.18 to 3.9 pN.

In contrast, *all* of the inextensible WLC models in Fig. 3 differ significantly from the experimental data. The curve for $P = 90$ nm agrees very closely with the experimental z/z_{max} ratio at $F = 3.9$ pN, but grossly overestimates the corresponding ratios at lower forces. The curves for $P = 50$, 44, and 38 nm all substantially underestimate the z/z_{max} ratios at the higher forces. The curve for $P = 44$ nm attains the minimum chisq by closely fitting the data at lower forces, whereas the curves for $P = 50$ and 38 nm overestimate and underestimate, respectively, the experimental values at lower forces. As noted previously [1], no single choice of P and z_{max} provides a satisfactory fit of the inextensible WLC model to all of the z/z_{max} data of Mosconi et al. [6] This conclusion differs from that of Marko and Siggia [73], who analyzed the data of Smith et al. [74] for a ~96.5 kbp DNA in 10 mM univalent salt, and obtained reasonably good agreement for an inextensible WLC model with $P = 53$ nm. It is noteworthy that the z_F/z_{max} data of Smith et al. in the low force regime, $F \leq 0.4$ pN, are not nearly as precise or finely spaced as those of Mosconi et al. [6], and in any case exhibit somewhat higher values in that range of primary interest.

4.2. C_{eff} vs. F

How well does the present two-state cooperative model agree with the measured torques of single twisted DNA molecules under tension, without invoking the previously assumed constant values for P and h? MN torque theory [71,72] expresses the reduced torque, $\tau_r = \tau/k_BT$, where τ is the torque, in terms of (i) the force, F;(ii) the excess twist per unit length, $\omega = (2\pi/((10.50)h_{av}))\sigma$, where σ is the superhelix density (excess turns per normal turn); (iii) the intrinsic torsional rigidity of the filament, C_{in}; (iv) P; (v)T; and (vi) τ_r (c.f. eq. 61 of ref. 72 or the particular rearrangement thereof in Eq.(1) of ref. [1]. The calculation proceeds by first reckoning the fraction, $f_b(F)$, of base-pairs in the b-state for an untwisted DNA subject to force, F, as described above, and from that computing the values of $h_{av}(F)$, $\alpha(F)$, $P(F)$, and $C_{in}(F) = h_{av}(F)\cdot\alpha(F)$. After inserting $h_{av}(F)$, $P(F)$, and $C_{in}(F)$ into the MN torque equation, and setting the superhelix density to 0.001 to enforce the small twist limit, that MN equation is solved for τ_r by using the Mathematica NSolve command and selecting the single purely real root. The effective torsional rigidity, C_{eff}, of the filament, which experiences both twist and writhe, is obtained from both experimental and theoretical reduced torques by the relation, $C_{eff}/k_BT = \tau_r/\omega$. Results for the two-state cooperative model are compared with two different kinds of experimental measurements in Fig. 4.

The theoretical curve in Fig. 4(A) is a reasonable compromise fit to three experimental data sets that differ somewhat from one another. A fourth experimental data set for considerably shorter (~3.4 kbp) DNAs was obtained by a somewhat different method [8], and lies a bit closer to the data of Mosconi et al. [6] It is not considered here, because of the increased importance of end-effects and possible interactions of such a short DNA with the surface of the magnetic bead to which it is attached. The continuation of the theoretical curve for the two-state model to higher forces yields, $Ceff = 411 \times 10^{-30}$ J m, at $F = 15$ pN, in good agreement with the experimental values ($(410 \pm 30$ and $440 \pm 40) \times 10^{-30}$ Jm) obtained by rotor bead assays [75]. At low forces the C_{eff} computed for the TWLC model (dotted line) substantially overestimates both the experimental values and those predicted by the two-state model, but at forces exceeding 4.0 pN, the two-state model predicts slightly higher values than the TWLC model, because the rise per bp of the former model extends somewhat beyond the 0.34 nm assumed for the TWLC model.

4.3. Increase in α upon circularization of 181 bp DNA

For a 181 bp linear DNA, the same two-state model with the same parameters in ~0.1 M NaCl at 293 K predicts $\alpha = 6.1 \times 10^{-19}$ J for the linear DNA in the absence of tension, and predicts for the circular form a tension, $F = 9.8$ pN, and torsion elastic constant, $\alpha = 10.1 \times 10^{-19}$ J. These agree reasonably well with the corresponding experimental values, $\alpha = (6.4 \pm 0.5)\text{x}10^{-19}$ J and $\alpha = (9.5 \pm 0.85) \times 10^{-19}$ J measured for the respective linear and circular 181 bp DNAs by the FPA method [76].

4.4. α determined from E_T of ~210 bp circular DNAs

From the combined topoisomer ratios of three circular DNAs containing 205, 207, and 217 bp of largely common sequence in ~30 mM univalent cations plus 10 mM Mg^{2+} at 310 K, the values, E_T = 3910 and 4068 were determined by Horowitz and Wang (HW) [65] using two different data analysis methods. After including estimated experimental errors, these values implied a range, $E_T \cong$ 3700–4200, as well as an average helix repeat of 10.54 bp/turn [65]. The average length of the three DNAs is 209.7 bp, and a DNA containing 210.8 bp would have exactly 20 turns. The two-state cooperative model is used to reckon directly E_T for a fictitious 210.8 bp DNA with a helix repeat of 10.81 bp/turn, corresponding to 19.5 turns for the linear DNA, and for which the two visible topoisomers would have linking differences of +0.5 and −0.5 turns. The calculation of E_T proceeds as described above in *Topoisomer distribution measurements and analyses* in Section 1 except that account is taken of the effect of the incorporated twist to shift the two-state equilibrium, as described in the Supporting Information I of ref. 2. The two-state cooperative model yields E_T = 3999, in excellent agreement with the experimental values of 3910 and 4068. The torsion elastic constant in the 210.8 bp circles was reckoned to be, $\alpha = 9.51 \times 10^{-19}$ J, which agrees well with the estimates, 9.53×10^{-19} J and 9.12×10^{-19} J obtained by previous analyses [63,64] of the reported value, E_T = 3910, using an inextensible TWLC model with assumed, h = 0.34 nm and P = 50 nm.

4.5. Mean rise per bp

The mean rise per bp of a linear DNA in 0.1 M NaCl at 293 K in the absence of force is predicted to be 0.325 nm, in reasonable agreement with the recent value, h_{av} = 0.323 ± 0.01 nm, reported for short synthetic 10–35 bp DNAs labeled with gold colloids [5].

4.6. κ_β^{II} and E_T of pUC19 and pBR322 DNAs

Of course, the two-state model with the parameters in Table 3 also predicts very well the κ_β^{II} values in Table 2, as indicated in Fig. 2, as well as the E_T values measured for the 2686 bp pUC19 DNA at various temperatures by GKV, which also appear in Table 2.

For a 4363 bp pBR322 DNA in ~35 mM univalent cations plus 10 mM Mg^{2+} at 310 K, the present two-state model predicts, E_T = 1140, which agrees well with the experimental values, E_T = 1130 ± 115 and 1155 ± 65, under the same conditions [65,77]. However, modestly lower experimental values, E_T = 986 ± 83, were repeatedly obtained for the 4932 bp p30δ DNA by precisely the same method [78,79]. Typically p30δ DNA is more readily equilibrated subsequent to relaxation of superhelical stress than is pBR322, which often displays extraordinarily long-lived metastability [77]. In any case, this modest, but statistically significant, difference between the E_T values of the two DNAs remains an unresolved mystery.

Overall, the present two-state cooperative model, in conjunction with Eqs.(9)–(10b) for the torsion elastic constants at zero pulling force under different conditions of temperature and ionic strength, does a remarkably good job of accounting for these diverse experimental test data without invoking extraneous assumptions about the value of P or h_{av}.

5. Origin of the premelting transition

Throughout the premelting region from 273 to 333 K, the UV absorbance and circular dichroism (CD) spectra of many, but not all, DNAs undergo substantial changes [17–24]. The magnitude of the positive CD band (ellipticity per mole of bases) at 273 nm increases with increasing T, whereas the magnitude of the negative band at 247 nm remains nearly unchanged. This behavior differs markedly from the change accompanying the DNA melting transition itself, wherein the positive and negative CD bands both decrease. This premelting transition is completely reversible and qualitatively, but not quantitatively, similar for DNAs from many sources, including phage, bacteria, salmon sperm, and calf-thymus. T-dependent changes in the Raman [25] and IR spectra [26] also accompany the premelting transition.

It was subsequently found that premelting transitions in the CD spectra of three different natural DNAs, including an 1876 bp *Hae*II restriction fragment of pBR322, were accompanied by substantial declines in their torsion elastic constants, α [16]. Also, DLS studies of the 1876 bp fragment at large scattering vector indicated that its bending elastic constant, κ_β, increased significantly over the premelting range from 293 to 333 K. Addition of 0.5 M tetramethyl-ammonium chloride (TMA), the cation of which is known to bind preferentially to AT-rich regions, substantially diminished these premelting changes in CD, α, and κ_β with increasing T.

The anti-correlated changes in α and κ_β associated with the premelting transition are in the same directions as the corresponding changes described above for the two-state cooperative model with increasing T, and occur over an overlapping range of temperatures. This suggests that the two-state cooperative structural transition is the likely origin of the premelting transition. This interpretation is supported by the presence of isosbestic points in the UV absorption difference spectra near 239 and 262 nm for T7 DNA at pH 7.6 in 0.1 M univalent cations at T = 276, 295, 308, 318, and 323 K [23]. These unusually precise difference spectra were measured using a dual beam instrument with the reference cell held at 276 K and the other cell at the desired T. Although the differences in absorbance are verysmall, <1% of the total absorbance at ~260 nm, the data are both smooth and consistent in regard to vibronic peaks and shoulders [23]. These spectra argue strongly for the presence of two different species with slightly different UV spectra, whose relative amounts vary with T. In addition, the rate of interconversion between states was quite slow at 276 K, as expected for a highly cooperative transition. When DNAs of different sequences were examined, the amplitudes of their difference spectra correlated surprisingly strongly with their pyrimidine-pyrimidine nearest-neighbor frequencies [23]. These coexisting states were originally tentatively suggested to be oligodC·oligodG subsequences that were either unprotonated or protonated, but that view waned, when subsequent studies revealed that polydC·polydG formed protonated triplexes at low pH, 4.0, but remained unprotonated duplex at and above neutral pH [80,81]. Moreover, direct alkaline titration of calf-thymus DNA revealed no consumption of OH^- whatsoever at a resolution better than 0.01 OH^- per DNA phosphate group between pH 7.8 and 10.3 [82]. In view of the foregoing, it seems likely that the isosbestic points arise from shifts of the $a \Leftrightarrow b$ equilibrium with increasing T. In that case, one could infer that mixed oligo pyrimidine and oligo purine subsequences favor the b state at or below ambient T, thereby providing a larger amplitude of change with rising temperature, which clearly favors the a state.

Upon increasing T, the absorbance between 239 nm and 262 nm decreases, whereas the absorbance at wavelengths beyond 262 nm increases. If the two states monitored by the absorption spectrum correspond to a and b, then these observations imply that the absorbance band of the a state favored by higher T is modestly red-shifted from that of the b state favored by lower T. This in turn suggests that the unexcited bases are in some sense farther apart in the a state, so as to be able to accommodate the instantaneously expanded electron cloud of an excited base at a lower energy cost than is the case for the b state. Greater separations likely imply weaker interactions between the unexcited bases, which would be consistent with the greater entropy of the a state that is responsible for its increasing prevalence with increasing T (Supporting Information II of ref. [2]).

If the premelting increase in CD at 273 nm reflects an increased fraction of bp in the a state with rising T, as required by the two-state model from the observed decrease in α with rising T, then a *decrease* in CD at 273 nm should accompany any perturbation that shifts the $a \Leftrightarrow b$ equilibrium toward the b state. Indeed, circularizing the aforementioned 181 bp DNA, which increased its α by 1.4-to 1.5-fold, presumably by increasing its fraction of bp in the b state, also decreased its

CD at 273 nm by ~0.9-fold, in qualitative agreement with this prediction.

If the premelting transition is due to shifting the two-state cooperative equilibrium toward the *a* state, as proposed, then the reported positive correlation between amplitudes of the changes in UV absorbance at 287 nm and CD at 273 nm with increasing temperature on one hand and increasing % AT on the other [23] suggests that certain AT-rich subsequences increasingly favor the (shorter, torsionally softer, flexurally stiffer) *a* state relative to the (longer, torsionally stiffer, flexurally softer) *b* state with rising temperature. Moreover, the presence of 0.5 M TMA appears to substantially inhibit the shift of the $a \Leftrightarrow b$ equilibrium toward the *a* state with increasing temperature [27]. This suggests that TMA cations prefer AT-rich sequences *in the b state* relative to those in the *a* state, and thereby help to stabilize the *b* state relative to the *a* state over the premelting range of *T*.

The range of temperatures (293–315 K) discussed above for the two-state model is much narrower than the full range of the premelting transition (273–333 K). The limited range of the two-state model examined here is not fundamental, but instead was adopted to ensure near constancy of various parameters of the model, such as the cooperativity parameter *J*, the difference in rise per bp δ, and the torsion (α_a and α_b) and bending ($\kappa_{\beta a}$ and $\kappa_{\beta b}$) elastic constants of the *a* and *b* states over the *T*-range considered. Over the much wider range of the premelting region, some or all of those parameters are likely to vary significantly with *T*. Thus, the same basic model, but with somewhat *T*-dependent parameters may well apply over the full premelting range, albeit with somewhat different parameters outside the 293–315 range. The intent here was to develop a model *with fixed parameters*, except for B_0, that applied over this limited 293–315 K range, where the vast majority of studies have been undertaken.

5.1. A possible explanation for the low and T-independent α-value of ϕ29 DNA

Linear ϕ29 DNA in ~100 mM univalent cations at 293 K exhibited the value, $\alpha = (4.55 \pm 0.4) \times 10^{-19}$ J [13,57], which is anomalously low compared to the values for plasmid DNAs, and it remained practically constant over the entire temperature range from 278 to 333 K [83]. Because this measured α-value is so close to α_a of the *a* state, the fraction of bp in the *a* state, $f_a = 0.955$, is already rather close to 1.0 at 293 K, so a *substantial* further shift of the a⇔b equilibrium toward the *a* state with increasing *T* is *not* possible. Hence, little or no premelting transition of its α is predicted by the two-state model, in agreement with the experiments [13,83]. Although the aspects of the ϕ29 sequence responsible for such a low α-value remain unknown, the 1097 bp insert fragment described in another study [84], provides a concrete example, wherein a small change in the sequence of a plasmid DNA has produced a similarly low α-value, so such low values are indeed possible for some sequences.

In 10 mM univalent cations at 293 K, ϕ29, M13mp7, and lambda DNAs all exhibit the same low value, $\alpha = (4.94 \pm 0.4) \times 10^{-19}$ J [13,57]. If the M13mp7 and lambda also follow ϕ29 in other regards, then M13mp7 and lambda are predicted to behave similarly to ϕ29 in 100 mM NaCl, exhibiting $\alpha = (4.55 \pm 0.4) \times 10^{-19}$ J, and remaining invariant as T increases from 283 K to 333 K. This prediction remains to be tested.

6. *T*-dependence of *P* from *j*-factor measurements

GKV reported *P*-values obtained from measured *j*-factors for ~200 bp DNAs in ~39 mM univalent cations plus 10 mM Mg^{2+} at various temperatures [15]. Those *P*-values decreased sufficiently rapidly with increasing *T* that the implied value of κ_β also decreased significantly with increasing *T*, in contrast to practically all other experiments. What are the predictions of the two-state model for the *T*-dependence of *P* inferred from *j*-factors of such small circles?

6.1. j-factors predicted by the two-state model

Calculation of persistence lengths from the two-state model to compare with those obtained from *j*-factor experiments proceeds in the following way. Certain properties of free unstrained DNAs in the ligation buffer at the prevailing 295 K are reckoned using the model parameters in Table 3, as follows. First, $\alpha_0 = 7.55 \times 10^{-19}$ J, is calculated from Eq.(9), and then $f_{b0} = 0.689$ is computed from Eq.(11), after which the equilibrium constant, B_0, for an isolated base-pair is reckoned by inverting Eq.(15), using the cooperativity parameter *J* from Table 3. The quantities, h_{av0}, $\kappa_{\beta 0}$, and P_0, are readily evaluated from f_{b0} via Eqs.(12) and (13), and $P_0 = h_{av0}\kappa_{\beta 0}/k_BT$. In the presence of a (not yet known) tensile force, *F*, acting along the axis of the circular DNA, the quantity B_F in Eq.(16) is altered to,

$$B_F = B_0 \exp[F\delta/k_BT] \tag{18}$$

After substituting B_F for B_0 in Eq.(15), the fraction $f_b(F)$ of base-pairs in the *b* state *in the presence of the axial tension* is expressed in terms of *F*. The mean rise per bp, $h_{av}(F)$, bending elastic constant, $\kappa_\beta(F)$, and persistence length, $P(F)$ are now also readily expressed in terms of *F*, B_0, and fixed parameters of the two-state model in Table 3 by Eqs.(12), (13), and (15) with $f_b(F)$ in place of f_b or $f_b(T)$. The bending rigidity of an elastic rod subject to an axial tensile force *F* is expressed in terms of *F* by,

$$A_F = h_{av}(F)\,\kappa_\beta(F) \tag{19}$$

Bending an elastic rod into a circle introduces an internal tensile force given by [2],

$$F = (A_F/2)\,(2\pi)^2/L_F{}^2 \tag{20}$$

where $L_F = N\,h_{av}(F)$ is the contour length of the DNA. In order to simplify the calculations, the number of bp employed at each temperature is chosen so that the linking difference vanishes (i.e. $\Delta L = 0$) under the prevailing conditions. (Excess twisting strain in a circular DNA with a non-integral number of turns affects the magnitude of B_0, but otherwise has no effect on the calculation of *F,* provided that the DNA remains close to a geometric circle. The calculation of B_0 in the presence of twisting strain was described in the Supporting Information I of ref. [2], but is not needed in this section.) When the various substitutions noted above are incorporated into Eq.(20), it becomes a transcendental equation for the unknown tensile force *F* in the circular DNA. This equation is solved numerically using Mathematica NestList and FixedPoint commands to determine the prevailing value, *F*, in the circular DNA. From this value of *F*, the values, B_F, $f_b(F)$, $h_{av}(F)$, $\kappa_\beta(F)$, $P(F)$, $A(F)$, and $\alpha(F)$ are readily calculated.

The *j*-factor is calculated by the method of Shimada and Yamakawa (SY) [85], which was developed for an *inextensible* wormlike filament with fixed bending and twisting rigidities. This theory can be applied directly to a filament that has been pre-extended to its final length by the tension in the circle, which in turn yields the final torsion and bending rigidities in the circular DNA. However, the resulting *j*-factor must be multiplied by the ratio of (fluctuated) extended DNAs to unextended DNAs in order to account fully for the work invested to attain the circular state. This ratio is just $p_{ext} = \exp(-NW/k_BT)$, where *W* is the integrated work to extend a single base-pair subunit by varying the force from 0 to *F*. *W* is given by,

$$W = \int_0^F x\,(df_b(x)/dx)\,\delta\,dx \tag{21}$$

and is evaluated numerically using the Mathematica NIntegrate command. The usual molar *j*-factor for an inextensible DNA with zero excess linking difference is reckoned according to,

$$j_M = ((10^{-3}\,8\pi^2\,c_0\,(L/2P)^{-6.5})/((2P)\,3\,n_{Av}))\exp[(-\pi^2/(L/2P)) + (c_1 + 0.25)\,(L/2P)] \tag{22a}$$

where

$$c_0 = 2.784\bullet(\alpha(F)/\kappa_\beta(F))^{0.5} \tag{22b}$$

$$c_1 = 0.2639 - (0.0383)\bullet(\alpha(F)/\kappa_\beta(F)) \quad (22c)$$

Eq.(22a) follows from Eqs.(1) and 37 of SY after multiplying by 10^{-3} to convert from units of m^{-3} to liter^{-1}. Eq.(22b–22c) follow from Eqs. (38) and (39) of SY for the case of zero linking difference and make use of constants from the first line of SY Table 1. The molar *j*-factor for the present extensible DNA is given by,

$$j_{Mext} = p_{ext}\bullet j_M \quad (23)$$

In order to compare with the *P* values obtained by GKV from their *j*-factor measurements, the computed j_{Mext} must be analyzed in the same way as was done by GKV for their experimental values. For this purpose, it is assumed that the DNA is inextensible with fixed rise per bp, $h = 0.34$ nm, and torsional rigidity, $C = 3.1 \times 10^{-28}$ J m, in Eqs. (22a–22c) (or equivalent protocol), and the persistence length, P_{GKV}, is determined by trial and error until the computed j_{MVV} matches j_{Mext}.

Values of j_{Mext} in Eq.(23) are computed at various temperatures from 278 to 342 K for the two-state cooperative transition model for DNAs with length *N* chosen to provide, $\Delta Lk = 0$, at each temperature examined [15,86]. Other parameters were taken from Table 3, as was done for $T = 295$ K in section (4) above. Then the value of *P* that would have been extracted by GKV from that j_{Mext} is determined by trial and error using $h = 0.34$ nm and $\alpha = 9.12 \times 10^{-19}$ ($C = 3.1 \times 10^{-28}$ J m) in Eqs.(22a–22c) at each temperature. That quantity is here designated as $P[j_{Mext}]_{GKV}$ at each *T*. The value of *P* reported by GKV is here designated as $P[j_{GKV}]_{GKV}$, and the *j*-factor reckoned from that value for the present DNA lengths with $\Delta Lk = 0$ is denoted here by j_{GKV}. These results are presented in Table 4.

Note that the predicted $\kappa_{\beta ext}$ increase slightly with increasing *T*, which follows the trend found for unstrained DNAs, despite the generation of axial tension and stretching caused by the bending strain in the circular DNAs.

The j_{Mext} values predicted by the two-state model increase much more slowly with increasing temperature than do the j_{GKV} values, and there is evidently a crossover at a temperature slightly above 303 K. Well below the crossover, j_{Mext} significantly exceeds j_{GKV}, and well above the crossover j_{GKV} significantly exceeds j_{Mext}. Consequently, the $P[j_{GKV}]_{GKV}$ values decline more rapidly with increasing *T* than do the $P[j_{Mext}]_{GKV}$ values, and there is a crossover at the same temperature as their respective *j*-factors.

The persistence lengths, P_{ext}, predicted by the two-state model for the circular DNAs decline slightly more rapidly with increasing *T* than do the $P[j_{Mext}]_{GKV}$, which are reckoned by assuming $h_0 = 0.34$ nm and $\alpha = 9.12 \times 10^{-19}$ J at every temperature. This is due to decreases in both α and h_{av} with increasing *T* in the two-state model DNA.

There arises now the question of whether the discrepancies between j_{Mext} and j_{GKV} are due to some *T*-dependent flaw in the two-state model, or instead to some *T*-dependent error in the experimental estimates of j_{GKV}, or to some flaw in the *j*-factor calculation, such as the assumed circular shape of the minimum energy conformation.

7. Critique of *j*-factor measurements

7.1. Problems associated with the ligation kinetics method

Particular problems with experimental *j*-factors obtained by the cyclization kinetics method and with theoretical predictions of *j*-factors based on a smooth (unkinked) circular ground state are discussed in Supplementary Information S5. It is concluded that neither the experiment nor the theory provides quantitatively reliable results.

A discussion of *j*-factor measurements by single molecule FRET is also provided in S5, and reaches a similar conclusion for both similar and different reasons.

In summary, neither the experimental j_{app} values of circular DNAs determined by the ligation kinetics method, nor the theoretical $j^{th}(\{\alpha,\kappa_\beta\}_{act})$ values can be regarded as unambiguous and quantitatively reliable. Under such circumstances, an unequivocal interpretation of the discrepancies between j_{Mext} and j_{GKV} values, or between $P[_{Mext]GKV}$ and $P_{[GKV]GKV}$ in Table 4 is not possible.

8. The meaning of the intrinsic bending and twisting elastic constant

Nomidis, Skoruppa, Carlon, and Marko (NSCM) [87] recently proved that the long-range effective intrinsic bending and twisting rigidities, *C* and *A*, of DNA are actually "renormalized" values for an underlying microscopic model that might also exhibit a non-vanishing twist-bend coupling term and/or anisotropy of the bending rigidity in its potential energy function. As a consequence of averaging the fluctuating thermal twists and bends that take place over a full turn of the helix, the microscopic model (under moderate tensions ≤ 20 pN) on distance scales exceeding a few turns behaves like an inextensible twisted wormlike coil (TWLC) of constant contour length with renormalized intrinsic elastic constants for twisting and bending, but *without* either twist-bend coupling or anisotropy of the renormalized bending potential! However, those renormalized rigidities, *C* and *A*, or equivalently, α and κ_β, depend upon the bare values of the twist-bend coupling constant and anisotropy of the bending as well as the bare twisting and bending elastic constants of the microscopic model according to a prescribed relation in each case, which is independent of the applied force or torque within typical experimental ranges [14,87].

Renormalized values, $\alpha = 10.9 \times 10^{-19}$ J ($C = 372 \times 10^{-30}$ Jm), and $\kappa_\beta = 5.2 \times 10^{-19}$ J ($A = 178 \times 10^{-30}$ Jm, equivalent to $P_{tot} = 44$ nm) at 293 K, were reckoned [14] from the bare elastic constants of the so-called oxDNA2 course-grained model, which includes both twist-bend coupling and bending anisotropy. Those bare elastic constants in turn were determined from correlated fluctuations in lengthy simulations of the oxDNA2 model potential [88]. After inserting these renormalized values into the MN torque formula, C_{eff} was calculated and compared with experimental data. Although the agreement was good at low forces, the computed C_{eff} values significantly underestimated the

Table 4
Values predicted by the two-state model for the persistence length, P_{ext}, bending elastic constant, $\kappa_{\beta ext}$, and *j*-factor, j_{Mext}, in the circular DNA with *N* chosen such that $\Delta Lk = 0$ at each prevailing temperature, *T*. Also presented are: (1) the persistence length, $P[j_{GKV}]_{GKV}$, reported by GKV in their Fig. 7, which was determined from their measured *j*-factor by using their fixed input constants, $h_0 = 0.34$ nm and $\alpha = 9.12 \times 10^{-19}$ J ($C = 3.1 \times 10^{-28}$ J m), in Eq.(22a–22c) or equivalent protocol; (2) the *j*-factor, j_{GKV}, that they would have measured for the hypothetical *N* such that $\Delta Lk = 0$, which is estimated here from their reported $P[j_{GKV}]_{GKV}$ by reversing the usual protocol; and (3) the persistence length, $P[j_{Mext}]_{GKV}$, determined from the computed j_{Mext} by using the above fixed input constants in Eq.(22a–22c).

T	*N* (bp)	P_{ext} (nm)	$\kappa_{\beta ext}$ x 10^{19} (J)	j_{Mext} (nM)	j_{GKV} (nM)	$P[j_{Mext}]_{GKV}$ (nm)	$P[j_{GKV}]_{GKV}$ (nm)
278	198.4	49.3	5.47	4.72	1.67	48.9	53.2
293	199.3	47.0	5.52	7.33	4.41	47.0	49.2
295	199.4	46.7	5.53	7.70	5.85	46.5	48.0
298	199.6	46.3	5.54	8.27	5.87	46.4	48.0
303	199.9	45.7	5.56	9.20	8.96	46.1	46.2
310	200.3	44.9	5.61	10.35	12.41	45.5	44.8
315	200.6	44.4	5.65	10.96	21.02	45.0	42.5

experimental values at all forces, $F \geq 1.75$ pN, so agreement was poor in that regard (c.f. Fig. 6 of ref.87). For example, the theoretical value, $C_{eff} = 350 \times 10^{-30}$ Jm, at $F = 15$ pN lies far below the reported experimental values (410 ± 30 and 440 ± 40) $\times 10^{-30}$ Jm at the same force [75]. These comparisons with experimental data supersede those in ref. 14, which were obtained by simulations using a subunit length (6.7 bp) that was too long to capture important averaging that takes place within a single turn of the helix. (E. Carlon, personal communication). In addition, because the renormalized constants define an inextensible TWLC model, they are also incapable of satisfactorily fitting the z/z_{max} vs. F data of Mosconi et al. for untwisted DNAs [6], as noted previously [1], and depicted in Fig. 3 above. These and other failures of inextensible TWLC models suggest that multi-conformation models, of which the two-state cooperative transition model is the simplest example, merit greater consideration.

9. Limitations of the two-state model

The present model should not be expected to apply under conditions outside the ranges of ionic strength, temperature, and tension considered here. For example, there is strong evidence that states with rather different properties from those of either *a* or *b* prevail in high concentrations (>1.0 M) of univalent cations [13,84], or in modest concentrations of multivalent ions [13], or in significant concentrations of ethylene glycol [89], or in ethanol and perhaps also other alcohols, including the crystallization solvent, 2-methyl-2,4-pentanediol, which apparently favor other structural families, such as the A and Z DNAs. The same caution applies also to DNAs in osmotically compressed hexagonal arrays.

The *a* and *b* states of the two-state model are not yet directly associated with any known structures at atomic level resolution, and it might be quite a while before they are. DNA crystals are typically grown from solutions under conditions far from those considered here, and in any case intermolecular forces in crystals do not adequately mimic the solution environment. Nuclear magnetic resonance (NMR) studies of DNA structures in solution so far have not provided structures with rises per bp as different as those of *a* and *b*. The coexistence of two right-handed helical duplex structures in solution for the same sequence has but rarely been reported in NMR studies [90]. However, it is mentionable that a great many of the short duplex oligomers, that were synthesized for structural investigation by NMR, exhibited 2-D spectra that were too complex for detailed structural analysis and were rejected as candidates for further study. For example, in the lab of the late Prof. Brian Reid, for every oligomer whose structure was further investigated in detail and reported, another ~25 short duplex oligomers were synthesized and their 2D spectra assayed and rejected. Given such a strong bias against systems of exhibiting complex NMR spectra, it is entirely expected that little or no information pertaining to both *a* and *b* states is found in the NMR structural databases.

10. Conclusions

The present study provides the first quantitative estimates of $\kappa_{\beta a}$ and $\kappa_{\beta b}$ for the respective *a* and *b* states of the two-state cooperative transition model. This model predicts the observed negative linear correlation between $1/\kappa_\beta$ and $1/\alpha$ as T is varied. With the 7 fixed parameters in Table 3 and knowledge of α at each temperature and ionic strength, this model yields quantitative or near quantitative agreement with numerous experimental data, including: (1) the mean rise per bp and also the difference in rise per bp between two coexisting states inferred from X-ray scattering measurements on gold-colloid-labeled DNAs with 10 to 35 bp; (2) the relative extension vs. force for a DNA with zero imposed twist from 0.18 to 3.9 pN; (3) the effective torsional rigidity vs. tension of a DNA from 0.2 to 15 pN; (4) the different torsion elastic constants of linear and circular forms of a 181 bp DNA at ambient T; (5) the effective torque constant E_T for supercoiling ~210 bp circular DNAs at 310 K; (6) the E_T for supercoiling 4363 bp pBR322 DNAs at ambient T; (7) the variation of the E_T for supercoiling a 2686 bp DNA with T over the range from 278 to 315 K. The proposed shift of the two-state equilibrium with increasing T is plausibly the origin of the broad premelting transition, and likely accounts for the reported isosbestic points in the T-dependent UV difference spectra.

Appendix A. Supplementary data

Supplementary data to this article can be found online at https://doi.org/10.1016/j.bpc.2019.106146.

References

[1] J.M. Schurr, A Possible Cooperative Structural Transition of DNA in the 0.25–2.0 pN Range, J. Phys. Chem. B 119 (2015) 6389–6400.
[2] J.M. Schurr, Possible origin of the increased torsion elastic constant of small circular DNAs: bending-induced axial tension, J. Phys. Chem. B *121* (2017) 5709–5717 (Correction to "Increased Torsion Elastic Constant of Small Circular DNAs: Bending-Induced Axial Tension". J. Phys. Chem. B 2017, 121, 10292).
[3] R.S. Mathew-Fenn, R. Das, P.A.B. Harbury, Remeasuring the double-helix, Science 322 (2008) 446–449.
[4] X. Shi, D. Herschlag, P.A. Harbury, Structural ensemble and microscopic elasticity of freely diffusing DNA by direct measurement of fluctuations, Proc. Natl. Acad. Sci. U. S. A. 110 (2013) E1444–E1451.
[5] T. Zettl, R.S. Mathew, S. Seifert, S. Doniach, P.A. Harbury, J. Lipfert, Absolute Intramolecular distance measurements with angstrom-resolution using anomalous small-angle X-ray scattering, Nano Lett. 16 (2017) 5353–5357.
[6] F. Mosconi, J.F. Allemand, D. Bensimon, V. Croquette, Measurement of the torque on a single stretched and twisted DNA using magnetic tweezers, Phys. Rev. Lett. 102 (2009) 078301–078304.
[7] J. Lipfert, W.J. Kerssemakers, T. Jager, N.H. Dekker, Magnetic torque tweezers: measuring torsional stiffness in DNA and RecA-DNA filaments, Nat. Methods 7 (2010) 977–980.
[8] J. Lipfert, M. Wiggin, J.W. Kerssemakers, F. Pedaci, N.H. Dekker, Freely orbiting magnetic tweezers to directly monitor changes in the twist of nucleic acids, Nat. Commun. *2* (2011) (439; Corrigendum, Nat. Commun. 2015, 6, 7192).
[9] A. Bolshoy, P. McNamara, R.E. Harrington, E.N. Trifonov, Curved DNA without A-A: experimental estimation of all 16 DNA wedge angles, Proc. Natl. Acad. Sci. U. S. A. 88 (1991) 2312–2316.
[10] W.K. Olson, A.A. Gorin, X.-J. Lu, L.M. Hock, V.B. Zhurkin, DNA sequence-dependent Deformabilitiy deduced from protein-DNA crystal complexes, Proc. Natl. Acad. Sci. U. S. A. 95 (1998) 11163–11168.
[11] J.A. Schellman, S.C. Harvey, Static contributions to the persistence length of DNA and dynamic contributions to DNA curvature, Biophys. Chem. 55 (1995) 95–115.
[12] J.M. Schurr, J.J. Delrow, B.S. Fujimoto, A.S. Benight, The question of long-range allosteric transitions in DNA, Biopolymers 44 (1997) 283–308.
[13] L. Song, Fluorescence Studies of Nucleic Acids: Dynamics, Rigidities, and Structures, in: J.M. Schurr, B.S. Fujimoto, P.-G. Wu, J.R. Lakowicz (Eds.), Topics in Fluorescence Spectroscopy, Vol. 3, Biochemical Applications, Plenum Press, New York, 1992, pp. 137–229.
[14] S.K. Nomidis, F. Kriegel, W. Vanderlinden, J. Lipfert, E. Carlon, Twist-Bend Coupling and the Torsional Response of Double-Stranded DNA, *Phys. Rev. Lett. 118* (2017) (217801–1—217801-6).
[15] S. Geggier, A. Kotlyar, A.V. Vologodskii, Temperature dependence of DNA persistence length, Nucleic Acids Res. 39 (2011) 1419–1426.
[16] J.J. Delrow, P.J. Heath, J.M. Schurr, On the origin of the temperature dependence of the supercoiling free energy, Biophys. J. 73 (1997) 2688–2701.
[17] J. Brahms, W.F.M. Mommaerts, A study of conformation of nucleic acids in solution by means of circular Dichroism, J. Mol. Biol. 10 (1964) 73–88.
[18] G. Luck, G. Zimmer, G. Snatzke, G. Söndgerath, Optical rotatory dispersion and circular Dichroism of DNA from various sources at alkaline pH, Eur. J. Biochem. 17 (1970) 514–522.
[19] R.B. Gennis, C.R. Cantor, Optical studies of a conformational change in DNA before melting, J. Mol. Biol. 65 (1972) 381–399.
[20] E. Palecek, I. Frick, Correlation between Polarographic reducibility and circular Dichroism of DNA at submelting temperatures, Biochem. Biophys. Res. Commun. 47 (1972) 1262–1269.
[21] D.S. Studdert, M. Patroni, R.C. Davis, Circular Dichroism of DNA: temperature and salt dependence, Biopolymers 11 (1972) 761–769.
[22] I.I. Ramm, V.I. Vorobev, T.M. Birshtein, I.A. Bolotina, M.V. Volkenstein, Circular Dichroism of DNA and histones in the Free State and in Deoxyribonucleoprotein, Eur. J. Biochem. 25 (1972) 245–253.
[23] M.T. Sarocchi, W. Guschlbauer, Protonated polynucleotide structures-Sequence and protonation-sensitive metastable states in DNA Premelting, Eur. J. Biochem. 34 (1973) 232–240.
[24] A.F. Usatyi, L.S. Shlyakhtenko, Temperature dependence of CD spectra of DNA from various sources, Biopolymers 12 (1973) 45–51.
[25] L. Rimai, V.M. Maher, D. Gill, I. Salmeen, J.J. McCormick, The temperature dependence of Raman intensities of DNA. Evidence for Premelting Changes and Correlations with Ultraviolet Spectra, Biochim. Biophys. Acta 361 (1974) 155–165.

[26] M. Shie, I.G. Kharitonenkov, T.I. Tikhonenko, Y.N. Chirgadze, New possibilities of investigating nucleic acids and nucleoproteins in aqueous solutions by infrared spectroscopy, Nature 235 (5338) (1972) 386–388.
[27] J.J. Delrow, P.J. Heath, B.S. Fujimoto, J.M. Schurr, Effect of Temperature on DNA Secondary Structure in the Absence and Presence of 0.5 M Tetramethylammonium Chloride, Biopolymers 45 (1998) 503–515.
[28] J. Bednar, P. Furrer, V. Katritch, A.Z. Stasiak, J. Dubochet, A. Stasiak, Determination of DNA persistence length by Cryo-Electron microscopy. Separation of the static and dynamic contributions to the apparent persistence length of DNA, J. Mol. Biol. 254 (1995) 579–594.
[29] M. Vologodskaia, A. Vologodskii, Contribution of the intrinsic curvature to measured DNA persistence length, J. Mol. Biol. 317 (2002) 205–213.
[30] H.B. Gray, J.E. Hearst, Flexibility of native DNA from the sedimentation behavior as a function of molecular weight and temperature, J. Mol. Biol. 35 (1968) 111–129.
[31] D. Pörschke, Persistence length and bending dynamics of DNA from electro-optical measurements at high salt concentrations, Biophys. Chem. 40 (1991) 169–179.
[32] P. Hagerman, B.H. Zimm, Monte Carlo approach to the analysis of the rotational diffusion of wormlike chains, Biopolymers 20 (1981) 1481–1502.
[33] M.M. Tirado, C. Lopez-Martinez, Garcia de la Torre, Comparison of theories for the rotational and translational diffusion coefficients of rod-like macromolecules. Application to short DNA fragments, J. Chem. Phys. 81 (1984) 2047–2051.
[34] S. Diekmann, W. Hillen, B. Morgenmeyer, R.D. Wells, D. Pörschke, Orientation relaxation of DNA restriction fragments and the internal mobility of the double Helix, Biophys. Chem. 15 (1982) 263–270.
[35] Y. Lu, B. Weers, N.C. Stellwagen, DNA Persistence Length Revisited, Biopolymers 61 (2002) 261–275.
[36] J. Newman, H.L. Swinney, L.A. Day, Hydrodynamic properties and structure of fd virus, J. Mol. Biol. 116 (1977) 593–606.
[37] J. Wilcoxon, J.M. Schurr, Temperature dependence of the dynamic light scattering of linear ϕ29 DNA, Biopolymers 22 (1983) 2273–2321.
[38] H. Yamakwa, M. Fujii, Translational diffusion coefficient of wormlike chains, Macromolecules 6 (1973) 407–415.
[39] D.R. Tree, A. Muralidhar, P.S. Doyle, K.D. Dorfman, Is DNA a good model polymer? Macromolecules 46 (2013) 8369–8382.
[40] R.P.C. Driessen, G. Sitters, N. Laurens, G.F. Moolenaar, G.J.L. Wuite, N. Goosen, R.Th. Dame, Effect of temperature on the intrinsic flexibility of DNA and its interaction with architectural proteins, Biochemistry 53 (2014) 6430–6438.
[41] A. Brunet, L. Salomé, P. Rousseau, N. Destainville, M. Manghi, C. Tardin, How does temperature impact the conformation of single DNA molecules below the melting temperature? Nucleic Acids Res. 46 (2017) 2074–2081.
[42] P.-G. Wu, L. Song, J.B. Clendenning, B.S. Fujimoto, A.S. Benight, J.M. Schurr, Interaction of chloroquine with linear and supercoiled DNAs. Effect on the torsional dynamics, rigidity, and twist energy parameter, Biochemistry 27 (1988) 8128–8144.
[43] A. Seidl, H.-J. Hinz, The free energy of DNA supercoiling is enthalpy determined, Proc. Natl. Acad. Sci. U. S. A. 81 (1984) 1312–1316.
[44] M. Duguet, The helical repeat of DNA at high temperature, Nucleic Acids Res. 21 (1993) 463–468.
[45] A.N. Naimushin, B.S. Fujimoto, J.M. Schurr, Dynamic bending rigidity of a 200-bp DNA in 4 mM ionic strength: a transient polarization grating study, Biophys. J. 78 (2000) 1498–1518.
[46] M. Hogan, J. Wang, R.H. Austin, C.L. Monitto, S. Hershkowitz, Molecular motion of DNA as measured by triplet anisotropy decay, Proc. Natl. Acad. Sci. U. S. A. 79 (1982) 3518–3522.
[47] S. Allison, R. Austin, M. Hogan, Bending and twisting dynamics of short linear DNAs. Analysis of the triplet anisotropy decay of a 209 base-pair fragment by Brownian simulations, J. Chem. Phys. 90 (1989) 3843–3854.
[48] A.N. Naimushin, B.S. Fujimoto, J.J. Delrow, J.M. Schurr, A transient polarization grating method to study tumbling and bending dynamics of DNA, Rev. Sci. Instrum. 70 (1999) 2471–2480.
[49] D. Pörschke, Structure and dynamics of double helices in solution: modes of DNA bending, J. Biomol. Struct. Dyn. 4 (1986) 373–389.
[50] Eden, D., Sunshine, C. Transient electric birefringence studies of bending thermodynamics and internal bending dynamics of short DNA restriction fragments. In Dynamic Behavior of Macromolecules, Colloids, Liquid Crystals and Biological Systems by Optical and Electro-0ptical Methods 1989, H. Watnabe, (editor (Hirokawa, Tokyo)).
[51] C. Elvingson, Computer simulation of the structure of DNA molecules in an electric field, Biophys. Chem. 43 (1992) 9–19.
[52] L. Song, S.A. Allison, J.M. Schurr, Normal mode theory for the Brownian dynamics of a weakly bending rod: comparison with Brownian dynamics simulations, Biopolymers 29 (1990) 1773–1791.
[53] L. Song, J.M. Schurr, Dynamic Bending Rigidity of DNA, Biopolymers 30 (1990) 229–237.
[54] T. Okonogi, A. Reese, S.C. Alley, P.B. Hopkins, B.H. Robinson, Flexibility of duplex DNA on the sub-microsecond timescale, Biophys. J. 77 (1999) 3256–3276.
[55] J.M. Schurr, Rotational diffusion of deformable macromolecules with mean local cylindrical symmetry, Chem. Phys. 84 (1984) 71–96.
[56] P.J. Heath, J.A. Gebe, S.A. Allison, J.M. Schurr, Comparison of analytical theory with Brownian dynamics simulations for small linear and circular DNAs, Macromolecules 29 (1996) 3583–3596.
[57] B.S. Fujimoto, J.M. Schurr, Dependence of the torsional rigidity of DNA on base composition, Nature 344 (1990) 175–178.
[58] V.V. Rybenkov, N.R. Cozzarelli, A.V. Vologodskii, Probability of DNA knotting and the effective diameter of the DNA double Helix, Proc. Natl. Acad. Sci. U. S. A. 90 (1993) 5307–5311.
[59] S.A. Rice, M. Nagasawa, Polyelectrolytes, vol. 2, Academic Press, New York, 1961 (pp. 131-185).
[60] J.J. Delrow, J.A. Gebe, J.M. Schurr, Comparison of hard-cylinder and screened coulomb interactions in the Modeling of supercoiled DNAs, Biopolymers 42 (1997) 455–470.
[61] D.C. Rau, V.A. Parsegian, Direct measurement of the intermolecular forces between Counterion-condensed DNA double helices, Biophys. J. 61 (1992) 246–259.
[62] A.N. Naimushin, N. Quach, B.S. Fujimoto, J.M. Schurr, Effect of polyethylene glycol on the supercoiling free energy of DNA, Biopolymers 58 (2001) 204–217.
[63] J. Shimada, H. Yamakawa, Statistical mechanics of DNA Topoisomers the helical worm-like chain, J. Mol. Biol. 184 (1985) 319–329.
[64] M.D. Frank-Kamenetskii, A.V. Lukashin, V.V. Anshelevich, A.V. Vologodskii, Torsional and bending rigidity of the double Helix from data on small DNA rings, J. Biomol. Struct. Dyn. 2 (1985) 1005–1012.
[65] D.S. Horowitz, J.C. Wang, Torsional rigidity of DNA and length dependence of the free energy of DNA supercoiling, J. Mol. Biol. 173 (1984) 75–91.
[66] J. Gore, Z. Bryant, M. Nollmann, M.U. Le, N.R. Cozzarelli, C. Bustamante, DNA overwinds when stretched, Nature 442 (2006) 836–839.
[67] T. Lionnet, S. Joubaud, R. Lavery, D. Bensimon, V. Croquette, Wringing out DNA, Phys. Rev. Lett. 96 (2006) (178102–1–178102-4).
[68] R.E. Depew, J.C. Wang, Conformational fluctuations of DNA Helix, Proc. Natl. Acad. Sci. U. S. A. 72 (1975) 4275–4279.
[69] F. Kriegel, C. Matek, T. Drsata, K. Kulenkampf, S. Tschirpke, M. Zacharias, F. Lankas, J. Lipfert, The temperature dependence of the helical twist of DNA, Nucleic Acids Res. 46 (2018) 7998–8009.
[70] C.A. Sucato, D.P. Rangel, D. Aspleaf, B.S. Fujimoto, J.M. Schurr, Monte Carlo simulations of locally melted supercoiled DNAs in 20 mM ionic strength, Biophys. J. 86 (1984) 3079–3098.
[71] J.D. Moroz, P. Nelson, Torsional directed walks, entropic elasticity, and DNA twist stiffness, Proc. Natl. Sci. USA 94 (1997) 14418–14422.
[72] J.D. Moroz, P. Nelson, Entropic Elasticity of Twist-Storing Polymers, Macromolecules 31 (1998) 6333–6347.
[73] J.F. Marko, E.D. Siggia, Stretching DNA, Macromolecules 28 (1995) 8759–8770.
[74] S.B. Smith, L. Finzi, C. Bustamante, Direct mechanical measurements of the elasticity of single DNA molecules by using magnetic beads, Science 258 (1992) 1122–1126.
[75] Z. Bryant, M.D. Stone, J. Gore, S.B. Smith, N.R. Cozzarelli, C. Bustamante, Structural transitions and elasticity from torque measurements on DNA, Nature 424 (2003) 338–341.
[76] P.J. Heath, J.B. Clendenning, B.S. Fujimoto, J.M. Schurr, Effect of bending strain on the torsion elastic constant of DNA, J. Mol. Biol. 260 (1996) 718–730.
[77] A.N. Naimushin, J.B. Clendenning, U.-S. Kim, L. Song, B.S. Fujimoto, D.W. Stewart, J.M. Schurr, Effect of Ethidium binding and Superhelix density on the apparent supercoiling free energy and torsion constant of pBR322 DNA, Biophys. Chem. 52 (1994) 219–226.
[78] J.B. Clendenning, A.N. Naimushin, B.S. Fujimoto, D.S. Stewart, J.M. Schurr, Effect of Ethidium binding and Superhelix density on the supercoiling free energy and torsion and bending constants of p30δ DNA, Biophys. Chem. 52 (1994) 191–218.
[79] G.P. Brewood, T. Aliwarga, J.M. Schurr, A Structural Transition in Duplex DNA Induced by Ethylene Glycol, J. Phys. Chem. B B2008 (112) (2008) 13367–13380.
[80] C. Marck, D. Thiele, C. Schneider, W. Guschlbauer, Protonated polynucleotides structures-22. CD study of the acid-base titration of poly(dG).poly(dC), Nucleic Acids Res. 5 (1978) 1979–1996.
[81] D. Thiele, C. Marck, C. Schneider, W. Guschlbauer, Protonated polynucleotides Structures-23. The Acid-Base hysteresis of poly(dG)•poly(dC), Nucleic Acids Res. 5 (1978) 1997–2012.
[82] S.-C. Lin, J.C. Thomas, S.A. Allison, J.M. Schurr, Dynamic light-scattering studies of internal motions in DNA. III. Evidence for titratable joints associated with bound polycations, Biopolymers 20 (1981) 209–230.
[83] J.C. Thomas, J.M. Schurr, Fluorescence depolarization and temperature dependence of the torsion elastic constant of linear ϕ29 deoxyribonucleic acid, Biochemistry 22 (1983) 6194–6198.
[84] U.-S. Kim, B.S. Fujimoto, C.E. Furlong, J.A. Sundstrom, R. Humbert, D.C. Teller, J.M. Schurr, Dynamics and structures of DNA: long-range effects of a 16 base-pair $(CG)_8$ sequence on secondary structure, Biopolymers 33 (1983) 1725–1745.
[85] J. Shimada, H. Yamakawa, Ring-closure probabilities for twisted wormlike chains. Application to DNA, Macromolecules 17 (1984) 689–698.
[86] V.V. Rybenkov, A.V. Vologodskii, N.R. Cozzrelli, The effect of ionic conditions on DNA helical repeat, effective diameter, and free energy of supercoiling, Nucleic Acids Res. 25 (1997) 1412–1418.
[87] Nomidis, S. K.; Skoruppa, E., Carlon, E. Marko, J. F. Twist-Bend Coupling and the Statistical Mechanics of DNA: Perturbation Theory and Beyond. Phys. Rev. E2019, 99, 032414-032429.
[88] E. Skoruppa, M. Laleman, S.K. Nomidis, E. Carlon, DNA Elasticity from coarse-grained simulations: The effect of groove asymmetry, J. Chem. Phys. *146* (2017), https://doi.org/10.1063/1.4984039 214902 (1–18).
[89] G.P. Brewood, J.J. Delrow, J.M. Schurr, Calf-thymus topoisomerase I equilibrates metastable secondary structure subsequent to relaxation of superhelical stress, Biochemistry 112 (2010) 3367–3380.
[90] D.G. Reid, S.A. Salisbury, T. Brown, D. Williams, Conformations of the two duplex forms of d(TCGA) in slow-exchange equilibrium characterized by NMR, Biochemistry 24 (1985) 4325–4332.